69-8024

YOUNG, Stephen James, 1942-
EMISSION CROSS SECTION MEASUREMENTS IN PROTON-NITROGEN COLLISIONS USING PHOTON COINCIDENCE TECHNIQUES.

University of Alaska, Ph.D., 1968
Physics, general

University Microfilms, Inc., Ann Arbor, Michigan

EMISSION CROSS SECTION MEASUREMENTS IN PROTON-NITROGEN COLLISIONS USING PHOTON COINCIDENCE TECHNIQUES

A

DISSERTATION

Presented to the Faculty of the
University of Alaska in Partial Fulfillment
of the Requirements
for the Degree of
DOCTOR OF PHILOSOPHY

by

Stephen James Young, B.S.

College, Alaska
May, 1968

EMISSION CROSS SECTION MEASUREMENTS IN PROTON-NITROGEN

COLLISIONS USING PHOTON COINCIDENCE TECHNIQUES

APPROVED:

G. D. Roberts

Albert F. Belon

Gerald J. Romick

Roger Sheridan
Chairman

Roger Sheridan
Department Head

APPROVED: C. Robl
Dean of the College of Mathematics,
Physical Sciences, and Engineering

DATE: April 29, 1968

E. Lee
Vice President for Research and
Advanced Study

ABSTRACT

The measurement of a cross section for the emission of a Balmer alpha (6563A) and N_2^+ (0,0) first negative band (3914A) photon from a hydrogen atom and an N_2^+ molecule which are excited simultaneously in the same $H^+ + N_2$ charge exchange collision has been performed in the proton velocity range from $.54 \times 10^8$ cm/sec (1.5 keV) to 2.40×10^8 cm/sec (30.2 keV). The measurement has been accomplished using the technique of photon-photon coincidence detection. Details of the technique are presented.

The simultaneous specification of the emissions (and hence final state excitations) of both systems produced in the collision makes this the first measurement of an emission cross section for a "well specified" charge exchange reaction.

The specific cross section measured is that for the emissions resulting from simultaneous excitation of the $B^2\Sigma_u^+$, $v' = 0$ state of N_2^+ and the 3p or 3d state of hydrogen. To within the random error associated with the experiment, the cross section has only a single-peak structure with a maximum value of $\sim 1.2 \times 10^{-18}$ cm^2 at a velocity of 1.15×10^8 cm/sec (6.9 keV).

The primary significant result of the investigation is the exceptionally good agreement in both shape and magnitude between the measured cross section and the cross section, σ_{uc}, calculated

on the assumption that the final state excitations of the two product systems are independent events. The average value of the ratio of the measured cross section to σ_{uc} for the twelve measured values of the cross section is 1.11±.34.

Secondary results are the remeasurement of the total cross section for the production of 3914A emission in $H^+ + N_2$ collisions showing good agreement with previous measurements and the redetermination of the total cross section for the production of Balmer alpha emission in the same type collisions showing varying degrees of agreement with previous measurements.

ACKNOWLEDGEMENTS

Since no worthwhile investigation is ever really accomplished by an individual without helpful suggestions, hints, or influences by others, I think it important to mention here a few of the persons who have provided especially useful assistance and guidance.

In the way of guidance, I especially acknowledge the help of my committee chairman Dr. Roger Sheridan who conceived the possibility of the present investigation and provided the insight necessary to overcome the sometimes seemingly insurmountable difficulties encountered in its development.

I wish also to acknowledge the helpful discussions and interest shown in this investigation by Dr. John Murray, Dr. Tom Roberts, Dr. Jerry Romick, Professor Al Belon, and Mr. Rudi Suchannek.

Special thanks are again due Dr. Murray for help in building, maintaining, and modifying the experimental apparatus, and Mr. Suchannek for designing and building the switching module.

Recognition is also due my wife Veronica who typed the first draft manuscripts and to the technical facilities of the Geophysical Institute for producing the final manuscript.

The work was performed under NSF Grant GP-5532 and personal financing was provided in part by the NASA trainee program.

TABLE OF CONTENTS

LIST OF FIGURES

CHAPTER I

INTRODUCTION

a) Introduction to the Problem

Charge exchange collisions between protons and neutral gas target systems (atoms or molecules) resulting in hydrogen atoms and ionic recoil systems are examples of atomic collisions in which both of the final systems have internal structure. The specification of a particular reaction in such collisions must necessarily then include a statement of the internal structural state of both product systems. In fact, if it is assumed that the initial state of the target system is given and that scattering is of no consequence to the results of the investigation (both assumptions being true in the present investigation), then the specifying of these two final states is in itself enough to define a unique reaction. Until recently, however, cross sections measured in such collisions have not been for specific reactions, but rather have been summations over the cross sections for all reactions that lead to a specified final state of only one system--the summation being implicit in the method of measurement.

For example, in charge exchange collisions resulting when a beam of protons is fired into a stationary target gas of N_2 molecules, the total cross section for the production of Balmer alpha emission is measured by counting the number of such photons emitted from a defined length of the beam per unit time. The emission of a Balmer alpha photon thus indicates that the final state of the hydrogen atom was one of the $n = 3$ states but says nothing about the final state of the resulting N_2^+ molecule. Similarly, the detection of N_2^+ band emissions implies only the excitation

of the final state of the N_2^+ molecule but gives no indication as to the final state of the resulting hydrogen atom. In fact, when observing N_2^+ band emissions excited by proton impact in actual experiments, there is no guarantee that a hydrogen atom is even produced--the excitation may be a result of simple ionization rather than charge exchange.

If $\sigma(i,j)$ is the cross section for the charge exchange reaction in which the hydrogen atom is excited to the $i^{\underline{th}}$ state and the N_2^+ molecule is excited to the $j^{\underline{th}}$ state, then the total cross section for exciting the hydrogen atom to the $i^{\underline{th}}$ state is

$$\sigma(i) = \sum_j \sigma(i,j)$$

and the total cross section for the emission of Balmer alpha radiation becomes

$$\sigma_\alpha = f_{3s}\sigma(3s) + f_{3p}\sigma(3p) + f_{3d}\sigma(3d)$$

$$= \sum_j \{f_{3s}\sigma(3s,j) + f_{3p}\sigma(3p,j) + f_{3d}\sigma(3d,j)\}$$

where f_{3s}, f_{3p}, and f_{3d} are the fraction of emissions from the 3s, 3p, and 3d states respectively that give Balmer alpha radiation. Use of the known transition probabilities for hydrogen (Condon and Shortley, 1963) gives $f_{3s} = 1$, $f_{3p} = .118$, and $f_{3d} = 1$.

Similarly, the total cross section for the emission of N_2^+ band photons in charge exchange collisions (say the (0,0)3914A band of the 1st negative system to be explicit) is

$$\sigma_{3914}^{ce} = \sum_i f_B \sigma(i,B)$$

where B represents the B $^2\Sigma_u^+, v' = 0$ state of N_2^+ and f_B is the fraction of molecules in this state that radiate so as to give 3914 band emissions. According to the data of Wallace and Nicholls (1955) and Nicholls (1962, 1963), $f_B = .705$.

It is apparent from the above discussion that, whereas cross sections such as σ_α and σ_{3914}^{ae} may be more useful in a practical application such as auroral analysis, the cross sections $\sigma(i,j)$ are the more fundamental in that they represent a unique reaction and in that other cross sections (σ_α and σ_{3914}^{ce} for example) may be determined from them. It is the measurement of this more fundamental cross section that is of concern here.

b) Statement of the Problem

In collisions between protons and nitrogen molecules, measurements of the total cross section for the production of Balmer alpha radiation have been made by Philpot and Hughes (1964), Sheridan and Clark (1965), and Murray et al. (1966) and the total cross section for the production of 3914 band radiation by Carleton and Lawrence (1958), Sheridan et al. (1961), Philpot and Hughes (1964), Sheridan and Clark (1965), Hughes and Doughty (1967), and Dahlberg et al. (1967). Note that this latter measured cross section includes contributions from both charge exchange-excitation (σ_{3914}^{ce}) and direct ionization-excitation (σ_{3914}^{i}) by the proton. The subject for study here is the cross section for the emission of Balmer alpha photons and 3914 band photons from systems (H and N_2^+) that are excited simultaneously into their proper upper states in the same charge exchange collision. If the cross section for the production of

these "partner" emissions for the case in which the hydrogen emission is produced by a transition from the 3m (m=s, p, or d) level is $\sigma_c(3m,B)$, then

$$\sigma_c(3m,B) = f_{3m}\, f_B\, \sigma(3m,B).$$

Symbolically, the three processes of interest are

$$H^+ + N_2(X^1\Sigma_g^+) \rightarrow H(n=3;\ \ell=0,1,2) + N_2^+(B^2\Sigma_u^+;v'=0)$$

$$\rightarrow H(n=2;\ell=0,1) + N_2^+\ (X^2\Sigma_g^+,\ v''=0) + h\nu_1 + h\nu_2$$

where the first arrow indicates the three charge exchange excitation reactions and the second arrow the subsequent emissions.

c) Method of Measurement

By virtue of the fact that the two emissions arise from systems that are excited at the same time and place, and since both excited states have finite lifetimes, there will be some kind of time and space correlation between the two emitted photons. The nature of these correlations will be considered more closely in Chapter II. Here it is sufficient to note that a situation exists that is well-suited for the method of coincidence detection. The principle of this technique is as follows: pulses arrive at the two inputs of the coincidence detector via two channels; if two pulses arrive at these two inputs within a time τ (the resolving time of the detector) of each other, an output pulse from the detector results; if the two pulses do not arrive within a time τ of each other, there is no output pulse. As applied to the investigation described here, the input pulses represent the detection of Balmer alpha and 3914 band photons by separate detectors. Thus,

when a reaction of interest occurs, a 3914 band photon and a Balmer alpha photon will be emitted as "partners." A certain fraction of these partner photons will be detected and will give rise to an output pulse from the coincidence detector. However, not every pulse out of the coincidence detector necessarily represents the occurrence of a reaction of the type under consideration. Account must be made of "accidental" coincidences.

Suppose, for example, that a collision takes place in which the hydrogen atom is excited to the n = 3 level but the N_2^+ molecule is not excited to the B state and that another collision takes place in which the hydrogen atom is not excited to the n = 3 level but the N_2^+ molecule is excited to the B state. Neither of these collisions is of interest, but it is still entirely possible for the hydrogen atom excited to the n = 3 level in one collision and the N_2^+ molecule excited to the B state in the other collision to emit Balmer alpha and 3914 band photons respectively within a time τ of each other thus effecting an output from the coincidence detector. This same accidental coincidence may occur between a photon detected by one photometer and a background or dark count from the other, or between dark counts from both photometers. Hence, the output from the coincidence detector is the sum of the "real" coincidences and the "accidental" coincidences. A method of separating the two is needed.

Since the accidental coincidences arise from input pulses that have no time correlation between themselves, the introduction of a time delay into one of the input channels can have no effect on the accidental coincidence counting rate. However, if the delay is much greater

than the average time between emissions of the two systems (a simple analysis gives that the average time between the emissions of two systems that are excited simultaneously is $\overline{(T_1-T_2)} = (\tau_1^2 + \tau_2^2)/(\tau_1 + \tau_2)$ where τ_1 and τ_2 are the lifetimes of the states), the time correlation between real events is destroyed. Hence, with the introduction of a delay, only the accidental coincidences are counted and the real coincidence counting rate is determined by subtraction of results obtained from measurements made with the delay in and out.

The preceding discussion can be given a somewhat more mathematical foundation. Consider a region of space in which there is a random source of events of type 1 of rate $\dot{N}_1$, a random source of events of type 2 of rate $\dot{N}_2$, and a random source of coincidence events (that is, events of type 1 and 2 that occur together with a definite correlation of some type) of rate $\dot{N}_R$. Let these events be detected by detectors D1 and D2 and the pulse outputs from these detectors be made incident on a coincidence detector D3 with resolving time τ. In addition, let a delay that can be switched in and out (of duration $t_D > \tau$) be introduced between D2 and D3 (or D1 and D3). To be specific about the nature of the correlation, assume that the events of type 1 and 2 in the coincidence source always occur within a time t_o of each other where $t_o < \tau$ (this to insure that all real coincidences are detected).

Then, in the case that $\dot{N}_1$, $\dot{N}_2$, and $\dot{N}_R$ are constants and that $\dot{N}_1\tau << 1$, $\dot{N}_2\tau << 1$, and $\dot{N}_R\tau << 1$, the coincidence counting rate when the delay is in will be (see for example Melissinos, 1966)

$$\dot{N}_c^{(in)} = 2\tau\,(\dot{N}_1 + \dot{N}_R)\,(\dot{N}_2 + \dot{N}_R)$$

since all of the pulses arriving at D3 from D1 and D2 are independent. When the delay is out, all pulses are independent except those originating from the coincidence source so that

$$\dot{N}_c^{(out)} = 2\tau [\dot{N}_1 \dot{N}_2 + \dot{N}_1 \dot{N}_R + \dot{N}_2 \dot{N}_R] + \dot{N}_R.$$

The difference is then

$$\dot{N}_c^{(out)} - \dot{N}_c^{(in)} = \dot{N}_R (1 - 2\tau \dot{N}_R) = \dot{N}_R$$

since $\tau \dot{N}_R << 1.$

As applied to the present investigation, $\dot{N}_1$ corresponds to the production of Balmer alpha photons from reactions not of interest, $\dot{N}_2$ to the production of 3914 band photons from reactions not of interest, and $\dot{N}_R$ to the production of both photons from reactions of interest. However, in the actual experimental situation, the assumption that the events from the coincidence source always occur within a time t_o of each other is not true for any finite value of t_o due to the finite lifetimes of the excited states. However, knowing the lifetimes of the states, the probability that the two events take place within some time T of each other can be calculated. Likewise, there can be no finite delay time t_D for which there is no real time correlation between the coincidence source singles events. But, a value of t_D can be chosen such that when the delay is greater than this value, the probability of detecting a real coincidence is arbitrarily small.

d) Previous Applications of the Coincidence Method

The coincidence detection technique has been used extensively since 1935 in both nuclear and high-energy experimentation. Its appearance in atomic physics, however, is fairly recent. The first application to atomic collision physics was made by Afrosimov et al. (1965) and more recently in the same line by Kessel and Everhart (1966). This work was concerned with the measurement of the differential scattering cross section for argon ions-on-argon in which the final "charge state," that is, degree of ionization, of both final products was specified.

Complications arise in this previous work which do not exist in the present investigation. In the previous work, only the degree of ionization of each of the product ions is specified and therefore the final states (in the exact sense of the word) are not explicitly known (other than is given by the fact that the product systems will most probably be in their ground states). The observation of particular emissions (as in the present investigation) however, uniquely defines the energy states of the final system. On the other hand, because of the very fact that the final states are determined by the resulting emissions, a basic complication arises. The complication is that the lifetimes associated with the exponential time decay of the excited states are comparable with the coincidence resolving time used. This complication is considered in the following chapter. A further complication in the previous work is that the final scattered and recoil particles do not necessarily move with the same speed after the

collision so that a delay (depending on the kinematics of the collision) has to be introduced in one or the other of the two detection channels to insure equal transit time for both events from the time of collision to the time of arrival at the coincidence detector. In the present application, the transit times of the two photons are necessarily the same since both photons travel the same distance.

The works of Afrosimov et al. and Kessel and Everhart (along with subsequent related work by the same authors) are essentially the only previous measurements of atomic collision cross sections in which the coincidence method is used. However, Cristofori et al. (1963) have used the method for calibration of a Lyman alpha detector by measuring coincidences between photons emitted in the sequence of events $H(n=3) \rightarrow H(n=2) \rightarrow H(n=1)$, and other work has been done in the investigation of secondary processes (Bogdanova and Marusin, 1966) and the investigation of photon correlations (Skachkov, 1964).

CHAPTER II

THEORY AND DESIGN OF THE EXPERIMENT

a) Signal

If $\sigma_c(3m,B)$ is the cross section for the production of a Balmer alpha photon from a hydrogen atom that is excited to the 3m state and a 3914 band photon from an N_2^+ molecule that is excited to the B state in the same charge exchange collision, then the number of such coincident emissions observed for a specific hydrogen transition (that is, $3s \longrightarrow 2p$, $3p \longrightarrow 2s$, or $3d \longrightarrow 2p$) per unit time is

$$\dot{N}_{3m} = \frac{INL}{e} A_1 A_2 P_{3m} \sigma_c(3m,B),$$

where $\dot{N}_{3m}$ is the number of detections per second, I is the proton current at the point of observation, N is the target gas number density and e is the electronic charge. A_1 and A_2 are the fractions of the number of photons emitted per unit volume which are detected by the respective detectors. These fractions depend on geometrical and optical transmission factors of the photometers and photometer efficiencies. L is the length of collision volume viewed, and P_{3m} is a factor that represents the limitation on detecting the reaction due to the coincidence method of detection. The factor P_{3m} is a function of the resolving time τ, the velocity of the proton beam v, and of L. Since the Balmer alpha emission consists of three separate lines of the same wavelength, the total number of counts observed per unit time is

$$\dot{N}_R = \frac{INL}{e} A_1 A_2 \left[P_{3s} \sigma_c(3s,B) + P_{3p} \sigma_c(3p,B) + P_{3d} \sigma_c(3d,B) \right].$$

b) Determination of P_{3m} Values

Let z be a measure of distance along the beam with z = 0 being defined as the position of observation. Consider a length of beam specified by a slit with edges at z = 0 and z = L > 0, and assume that the excitation process occurs in the region 0 < z < L. The function P_{3m} is then the probability that the emissions from the two systems in their excited states occur within a time τ of each other and in view (that is, in the above defined region). Since it is assumed that the excitation collision takes place in this region, the probability that it does so at a time $0 < t_o < L/v$ in a time interval dt_o ($t=0$ is defined as the time when the proton causing the reaction reaches position $z=0$) is

$$dp_o = \frac{dt_o}{(L/v)}$$

assuming that L is short enough that the beam current is constant in this region.

If the excitation takes place at time t_o, then the probability that the moving system (denoted by subscript M) emits a photon at a time $t_M \geq t_o$ in a time interval dt_M is

$$dp_M = \frac{1}{\tau_M} e^{-(t_M - t_o)/\tau_M} \, dt_M$$

where τ_M is the lifetime of the excited state of the moving system. Similarly, the probability that the "stationary" recoil system (denoted by subscript S) emits a photon at a time $t_S \geq t_o$ in a time interval dt_S is

$$dp_S = \frac{1}{\tau_S} e^{-(t_S - t_o)/\tau_S} \, dt_S.$$

Note that since $\sigma_c(3m,B)$ is defined as an emission cross section, dp_M and dp_S need not be multiplied by additional factors representing the fraction of emissions from the excited states that have the required wavelength.

That the recoil system may be considered as stationary results from the fact that the initial target velocities are only thermal, and that in charge exchange collisions of this type, little momentum is transferred to the recoil particle.

The probability P_{3m} is the product $dp_o dp_M dp_S$ integrated over suitable limits. Observing that the moving system must emit within the viewing region in order that its emission be seen, the limits on the variable t_M are

$$t_o \leq t_M \leq L/v.$$

The limits on the stationary system are then set by the requirement that in order for the reaction to be detected, the time interval between emissions must be less than τ. Hence, in the case that $\tau \geq L/v$, the limits on the variable t_S are

$$t_o \leq t_S \leq t_M + \tau.$$

The limits on the variable t_o are

$$0 \leq t_o \leq L/v.$$

Hence,

$$P_{3m} = \int_{t_o=0}^{L/v} \int_{t_M=t_o}^{L/v} \int_{t_S=t_o}^{t_M+\tau} dp_S dp_M dp_o$$

with the result that

$$P_{3m}(\tau,L,v) = 1 - \frac{\tau_S}{\tau_S+\tau_M}\exp(-\tau/\tau_S) + (v/L)\left[\frac{\tau_S^2\tau_M}{(\tau_S+\tau_M)^2}\left\{1 - \exp\left(-\frac{L}{v}\left\{\frac{\tau_S+\tau_M}{\tau_S\tau_M}\right\}\right)\right\}\exp(-\tau/\tau_S) - \tau_S\left\{1 - \exp(-L/v\tau_M)\right\}\right].$$

Notice that P_{3m} involves the variables L and v only as the ratio L/v.

The specialization to the case where $\tau \geq L/v$ results from the fact that the maximum value of L/v used in this experiment is on the order of 30 nsec, and a later calculation will show that the optimum value of τ to be used is on the order of 70 nsec. The P_{3m} functions are plotted in Figure 1 for m=s,d, and p as a function of L/v to indicate their shapes and relative values. The values of τ_M are 160 nsec, 15.6 nsec, and 5.4 nsec respectively for m=s,d,p (Condon and Shortley, 1963) and τ_S = 65.8 nsec (Bennett and Dalby, 1959). The value of τ is 70 nsec.

Two additional assumptions have been made in this derivation that need some explanation. It has been assumed that each portion of the beam within the collision region is seen with equal efficiency by the detectors. However, distortions in the optical detection may cause one part of the beam to be seen less (or more) efficiently than another part. If $A_S(z)$ and $A_M(z)$ are the efficiency functions for the 3914 band photon and Balmer alpha photon detectors respectively, where $A_S(z) = A_M(z) = 0$ outside the viewing region and both are normalized to 1 at the most efficient position within the viewing region, then P_{3m} is modified to read

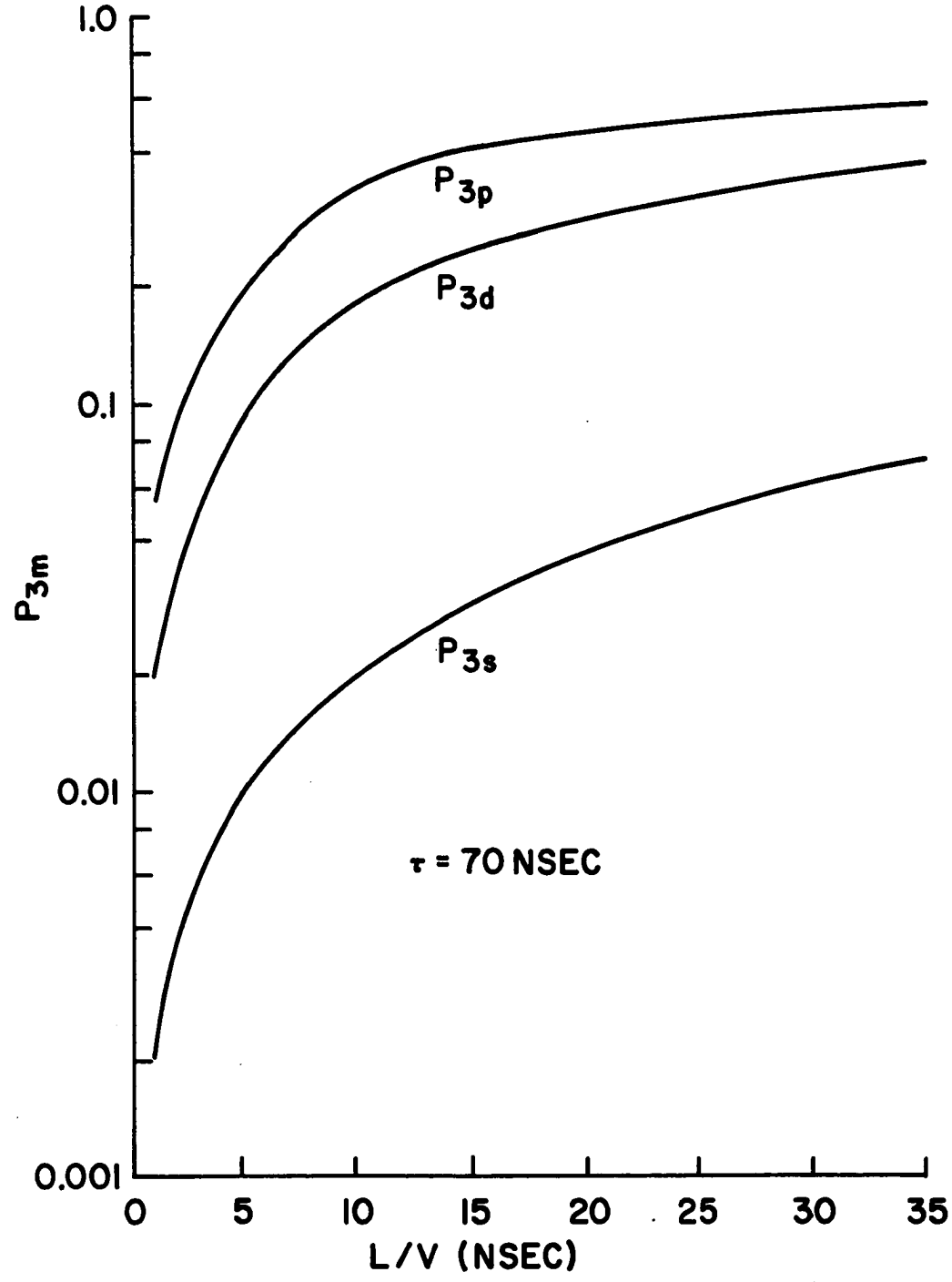

P_{3m} PROBABILITY FACTORS

FIGURE 1

$$P_{3m} = \int_{t_o=0}^{L/v} \int_{t_M=t_o}^{L/v} \int_{t_s=t_o}^{t_M+\tau} A_S(vt_o)A_M(vt_M)dp_S dp_M dp_o.$$

In the case that $A_S(z)$ and $A_M(z)$ are square functions, this expression for P_{3m} of course reduces to the previous expression. This correction has been neglected in this first order derivation.

The other assumption is related to the "jitter" in the detection and pulse shaping electronics--that is, the transit time from the emission of a photon to the arrival of the resulting pulse at the coincidence detector is not necessarily a constant but may have a distribution about some average value. Because of this effect, two photons which are emitted such that $|t_M-t_S|$ is less than but nearly equal to τ may result in pulses that arrive at the coincidence detector with a time difference somewhat greater than τ and hence are not detected in coincidence. Similarly, emissions which occur with $|t_M-t_S|$ just greater than τ, and which therefore should not be detected in coincidence, may be detected. If $C(\tau_d)$ is the probability that the two emissions will be detected in coincidence when their time difference is τ_d, the P_{3m} must be further modified to read (with the nonequality of efficiency included)

$$P_{3m} = \int_{t_o=0}^{L/v} \int_{t_M=t_o}^{L/v} \int_{t_S=t_o}^{\infty} A_S(vt_o)A_M(vt_M)C(t_S-t_M)dp_S dp_M dp_o.$$

If there is no jitter, then

$$C(\tau_d) = \begin{cases} 0 & \tau_d < -\tau \\ 1 & -\tau \leq \tau_d \leq \tau \\ 0 & \tau < \tau_d \end{cases}$$

and the expression becomes the same as that including the A(z) corrections only. The jitter can affect only those pulses for which $\tau_d = \pm\tau \pm \tau_j$ where τ_j is the width of the jitter, and if τ_j is small compared with the width 2τ (in this case, $\tau_j/2\tau \approx .02$), then only a small error can result from its exclusion from the expression for P_{3m}.

c) Neglect of the 3s→2p Contribution to the Signal

From Figure 1 it is seen that the relative probability of detecting the reaction is small if the hydrogen atom emits by the 3s→2p mode. This suggests that this contribution to the signal may be neglected if the $\sigma_c(3s,B)$ cross section is not too large. If it is no larger than that given by the assumption that the cross sections $\sigma_c(3m,B)$ for different m have the same shape and relative sizes among themselves as do the corresponding total cross sections for the production of Balmer alpha emissions, σ_{3m}, then it is possible to determine the proton velocity range for which this contribution may be neglected. Using the σ_{3s} cross section reported by Hughes et al. (1966) and Hughes et al. (1967) and the total Balmer alpha cross section of Murray et al. (1966), it is found that the contribution to the signal from 3s→2p transitions (Figure 2), that is, the quantity $P_{3s}\sigma_c(3s,B)$, is less than a tenth of the total contribution for proton velocities less than about 1.85×10^8 cm/sec for the worst

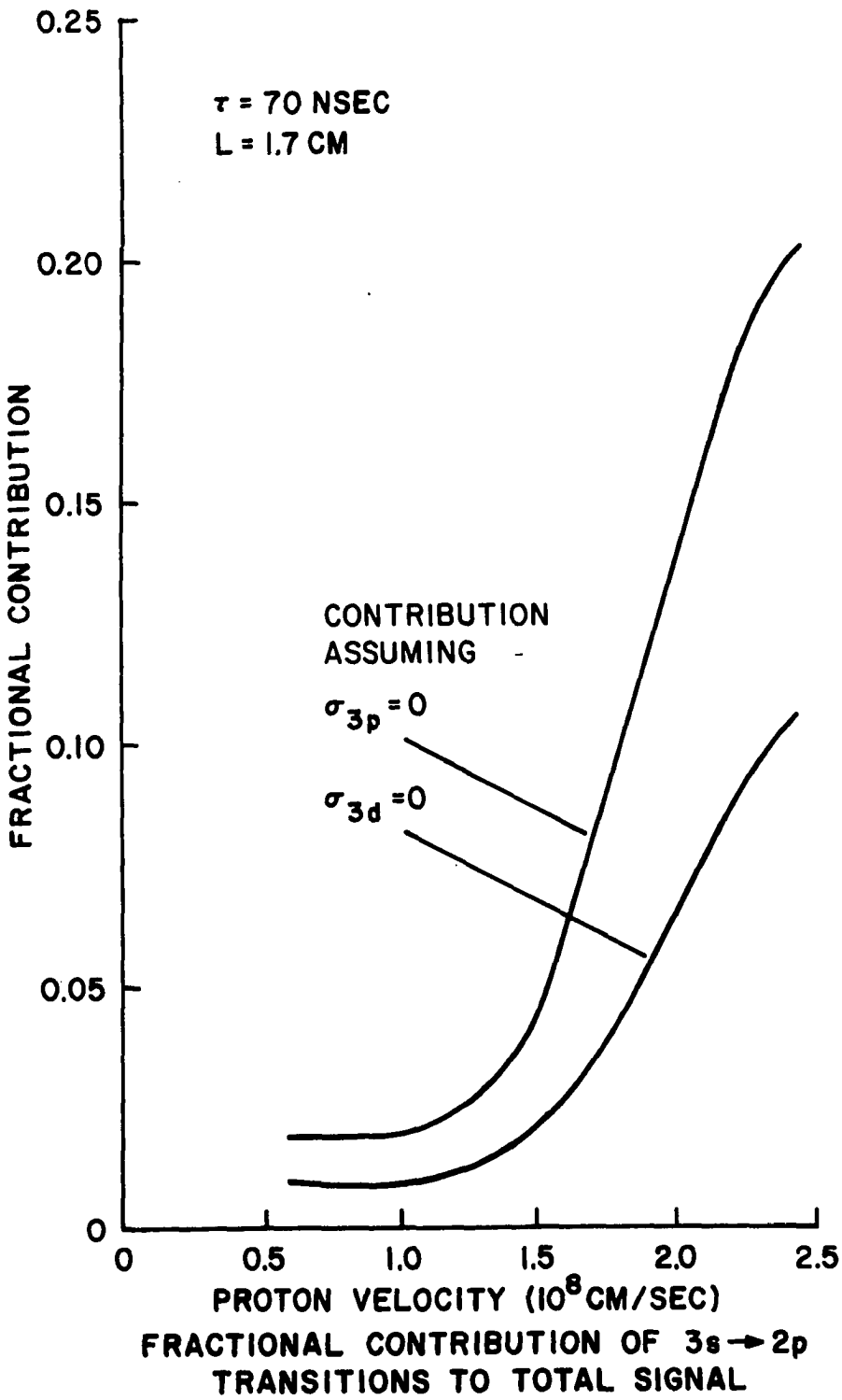

FRACTIONAL CONTRIBUTION OF 3s → 2p TRANSITIONS TO TOTAL SIGNAL

FIGURE 2

case of assumed ratio between σ_{3p} and σ_{3d}, (that is, for $\sigma_{3p}=0$). The basis of the above assumption on the relative sizes of the cross sections will be discussed more fully in Chapter V.

d) Cascade Contribution

The contribution to signal from cascade population of upper levels can become significant in measurements of total cross sections such as σ_α (Murray, 1968). Since the effective lifetimes of cascade processes are necessarily longer than for direct excitation, however, the contribution is less when measuring with the coincidence method because of the time correlation discrimination. The significance of 1^{st} order cascade in hydrogen, that is direct excitation to levels higher than the n=3 level with a single cascade transition to the n=3 level, can be estimated from the knowledge of (1) the cross sections for capture into these higher levels, (2) the probability that the cascade route to the n=3 level will be followed (for 1^{st} order cascade this is simply the ratio of the transition probability from the higher level to the n=3 level to the total transition probability from the higher level), and (3) the probability that the two emissions occur within a time τ of each other and in view. This latter factor may be calculated as in section b but with dp_M replaced by

$$dp_M = \frac{1}{\tau_M(1-\gamma)} \left\{ \exp\left(- \frac{t_M - t_o}{\tau_M} \right) - \exp\left(- \frac{t_M - t_o}{\gamma \tau_M} \right) \right\} dt_M$$

where $\gamma = \tau_u/\tau_M$ and where τ_u is the lifetime of the higher level. The quantity dp_M is the probability that the Balmer alpha photon is emitted at time t_M in dt_M if the level u is populated at time t_o and makes a

transition to the n=3 level. Again, as in section b, dp_M is not multiplied by an additional factor representing the fraction of atoms in the n=3 level making the correct transition. This gives the result that

$$P_{3m}^{cas}(\tau) = 1 - \frac{e^{-\alpha}}{(1-\gamma)}\left\{\frac{1}{(1+\beta)} - \frac{\gamma}{(1+\gamma\beta)}\right\} + \frac{\beta}{(1-\gamma)\theta}\left[(\gamma^2-1)\right.$$

$$+ e^{-\alpha}\left\{\frac{1}{(1+\beta)^2} - \frac{\gamma^2}{(1+\gamma\beta)^2}\right\} + \left\{e^{-\theta/\beta} - \gamma^2 e^{-\theta/\beta\gamma}\right\}$$

$$\left. - e^{-\alpha}\left\{\frac{1}{(1+\beta)^2}\, e^{-\theta(\frac{1+\beta}{\beta})} - \frac{\gamma^2}{(1+\gamma\beta)^2}\, e^{-\theta(\frac{1+\gamma\beta}{\gamma\beta})}\right\}\right]$$

where $\beta = \tau_M/\tau_S$, $\alpha = \tau/\tau_S$, and $\theta = L/v\tau_S$.

The quantity $[A(u\rightarrow 3m)/A(u)]\, P_{3m}^{cas}$ is plotted in Figure 3 for some of the possibly important upper levels. The value of τ is 70 nsec.

Considering only 1st order cascade from the n=4 and n=5 levels, it can be shown that the worst possible case of cascade contribution results if all capture into these levels occurs into the d states. In this case, using the Balmer beta emission cross section of Carleton and Lawrence (1958) and the ratio between the Balmer beta and Balmer gamma emission cross sections reported by Bobashev et al. (1964) for protons incident on neon, one finds that the cascade contribution to the signal is of the same order as for the 3s→2p direct excitation contribution. Since this is a worst case estimate and since the 3s→2p contribution has been shown to be negligible over most of the velocity range used,

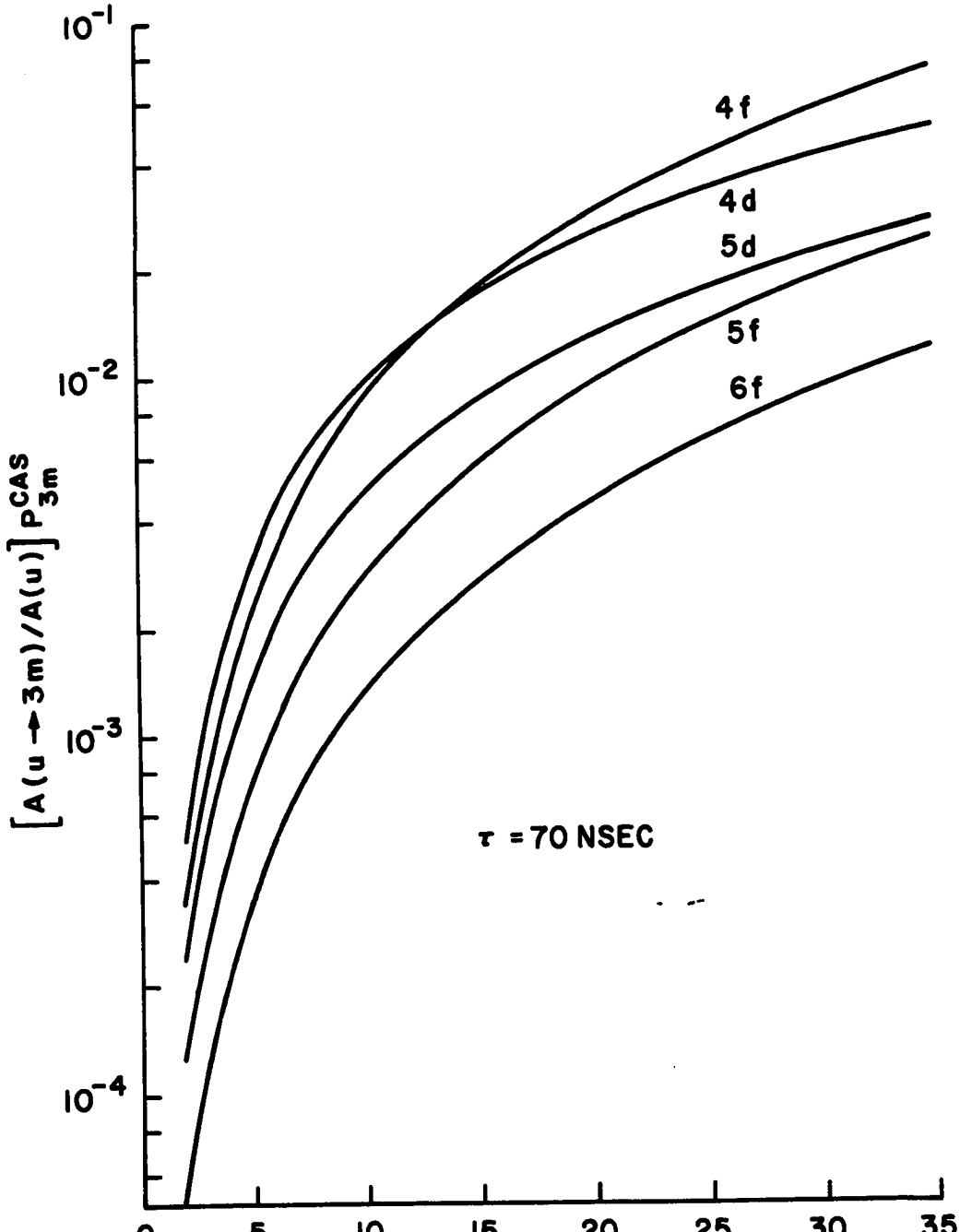

CASCADE PROBABILITY FUNCTIONS

FIGURE 3

cascade contribution has also been neglected. Contributions to the signal from cascade processes in N_2^+ have also been neglected since, although there are states above the B state which may make transitions to the B state, emissions resulting from these transitions have never been observed.

e) Resolution of Cross Sections

Having established that the 3s→2p and cascade contribution to the signal may be neglected, the total number of counts observed per unit time will then be approximately

$$\dot{N}_R = \frac{INL}{e} A_1 A_2 \left[P_{3p}(\tau, L/v)\sigma_c(3p,B) + P_{3d}(\tau, L/v)\sigma_c(3d,B) \right]$$

or

$$G = P_{3p}\sigma_c(3p,B) + P_{3d}\sigma_c(3d,B)$$

where

$$G = \frac{\dot{N}_R e}{INL\ A_1 A_2} .$$

The most straightforward method of obtaining values for $\sigma_c(3p,B)$ and $\sigma_c(3d,B)$ would be to measure G for two different values of τ (at the same velocity) and to solve the set of equations

$$G_1 = P_{3p}(\tau_1)\sigma_c(3p,B) + P_{3d}(\tau_1)\sigma_c(3d,B)$$

$$G_2 = P_{3p}(\tau_2)\sigma_c(3p,B) + P_{3d}(\tau_2)\sigma_c(3d,B).$$

Unfortunately, the inversion determinate

$$\Delta = \begin{vmatrix} P_{3p}(\tau_1) & P_{3d}(\tau_1) \\ P_{3p}(\tau_2) & P_{3d}(\tau_2) \end{vmatrix}$$

is almost identically zero for all variations of τ so that the equations are degenerate.

A variation in L could in principle lead to non-degenerate equations, that is

$$G_1' = L_1 \left[P_{3p}(L_1)\sigma_c(3p,B) + P_{3d}(L_1)\sigma_c(3d,B) \right]$$

$$G_2' = L_2 \left[P_{3p}(L_2)\sigma_c(3p,B) + P_{3d}(L_2)\sigma_c(3d,B) \right]$$

where

$$G' = \frac{\dot{N}_R e}{INA_1A_2}$$

and where

$$\Delta' = \begin{vmatrix} P_{3p}(L_1) & P_{3d}(L_1) \\ P_{3p}(L_2) & P_{3d}(L_2) \end{vmatrix} \neq 0$$

However, the accuracy required in the measurement of G_1' and G_2' to give $\sigma_c(3p,B)$ and $\sigma_c(3d,B)$ to within even 50% is well outside the capabilities of this experiment. Calculations show that to get a value of $\sigma_c(3p,B)$ or $\sigma_c(3d,B)$ to within this value would require a signal to noise ratio in the measurement of G' on the order of 30. As is demonstrated in section g of this chapter, this value is well above any that could be expected from this experiment in a reasonable length of time.

f) Approximation to $\sigma_c(3p,B) + \sigma_c(3d,B)$

The results of the last section indicate that there is little hope of experimentally resolving the measured quantity $P_{3p}\sigma_c(3p,B)+P_{3d}\sigma_c(3d,B)$ into the individual cross sections $\sigma_c(3p,B)$ and $\sigma_c(3d,B)$ in this experiment. Another method of obtaining meaningful results from the measured signal is to ask how closely a measurement of G could determine the direct sum of the cross sections, $\sigma_c(3p,B)+\sigma_c(3d,B)$. Although P_{3p} and P_{3d} are not equal (nor do they form a constant ratio) as a function of proton velocity for a fixed value of τ, Figure 4 shows that the ratio of these two probabilities in the L/v range of interest is not more than about 2 and does not change by more than a factor of 1.5. This suggests that the function

$$\frac{G}{\frac{1}{2}(P_{3p} + P_{3d})} \equiv \frac{G}{P_e}$$

may give a fairly reliable indication of the magnitude of the direct sum. The absolute value of the fractional difference between this function and the direct sum is plotted in Figure 5 as a function of the ratio

$$R = \frac{\sigma_c(3p,B)}{\sigma_c(3d,B)} \quad \text{or} \quad \left(= \frac{\sigma_c(3d,B)}{\sigma_c(3p,B)} \right)$$

for various values of L/v. The value of τ is again 70 nsec. In the worst possible case, that is, where one of the cross sections is zero (and hence $R=\infty$), the maximum error in the assertion that

$$\frac{G}{P_e} = \sigma_c(3p,B) + \sigma_c(3d,B)$$

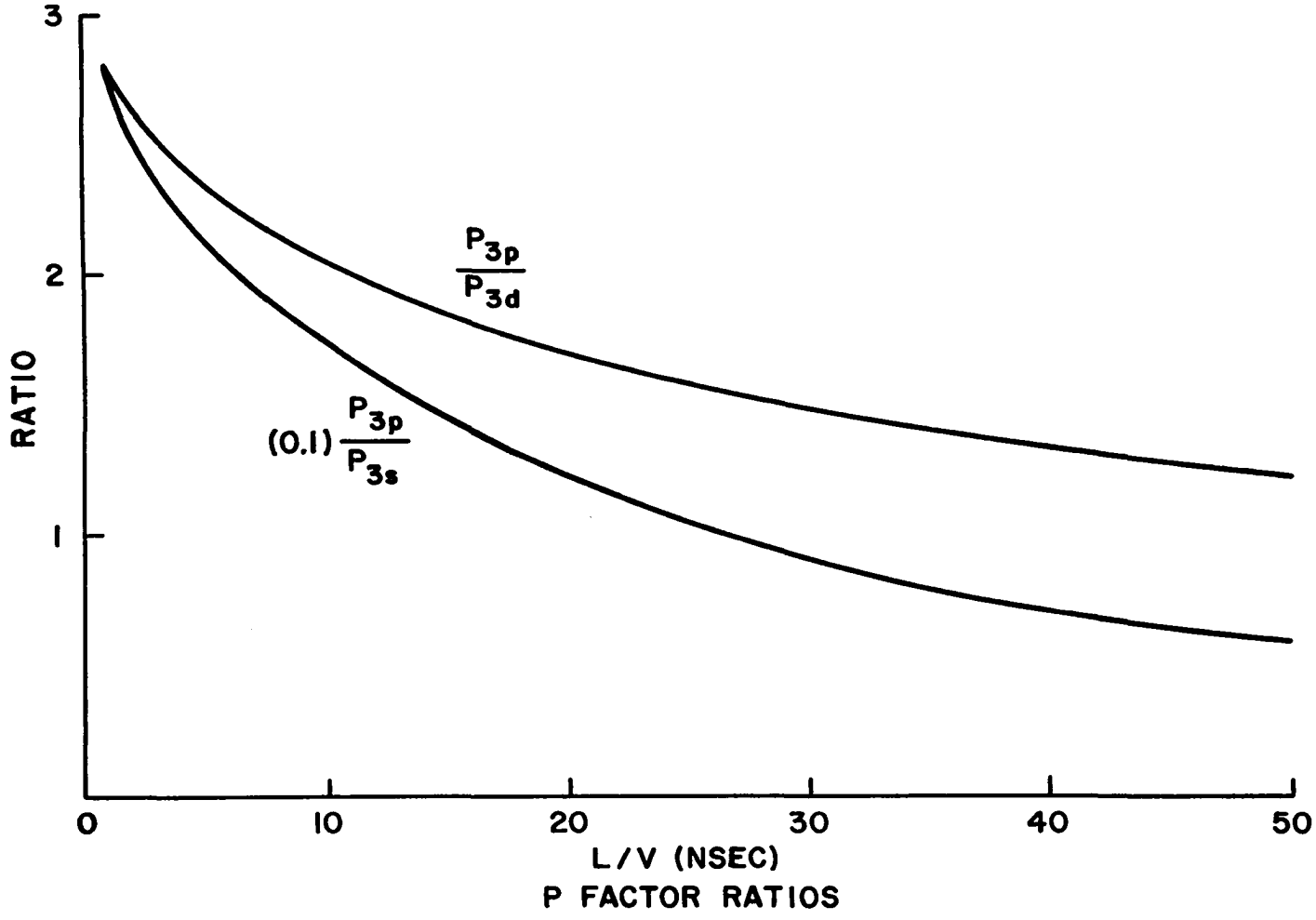

FIGURE 4

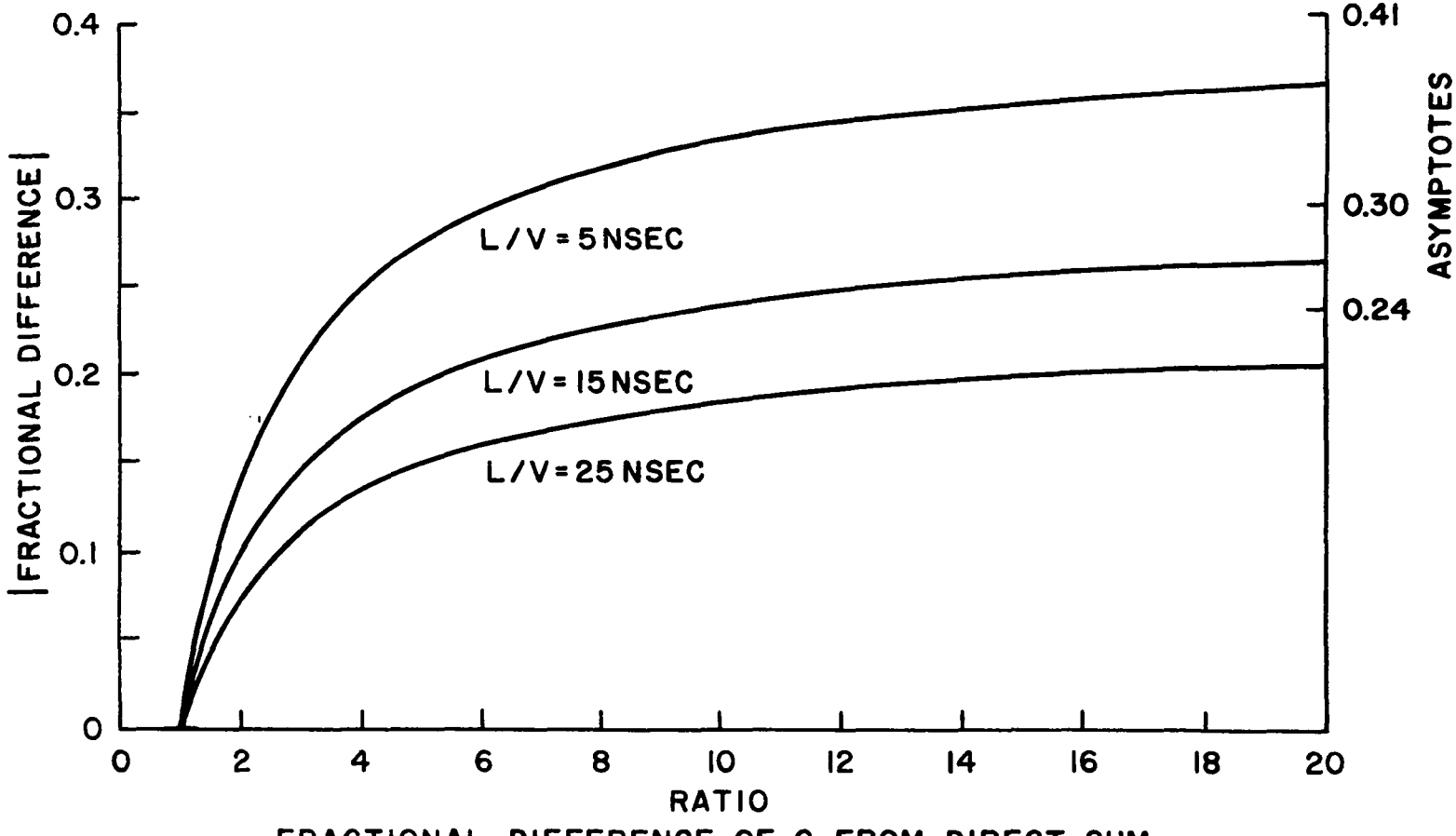

FRACTIONAL DIFFERENCE OF G FROM DIRECT SUM

FIGURE 5

is about 40% at the higher velocities and about 20% at the lower velocities. However, again using the assumption on the relative sizes of the cross sections as was used in section c, indications by Hughes and Doughty (1967) and Bates and Dalgarno (1953) suggest that the ratio is no greater than 3 in most of the L/v range used here (and much less at some velocities) so that the maximum error in this case is on the order of 20% at the higher velocities and about 10% at the lower velocities. Since this is the order of the accuracy of the experiment, this approximation seems appropriate and is used to obtain the final result given here.

g) Signal to Noise Ratio (STN)

It has already been indicated that the limitation in the accuracy of this experiment is set by the signal to noise ratio. The noise is defined as the root mean square deviation of the signal and, if ideal counting statistics apply, is given by the square root of the total number of counts received in an integrating time T. The signal is, of course, the number of real counts detected in the time T.

The counting rates from the individual detectors are

$$\dot{N}_H = kA_1Q$$

$$\dot{N}_N = kA_2\sigma_{3914}$$

where Q is the "effective" total cross section for the production of Balmer alpha photons (see section d, Chapter IV), σ_{3914} is the total cross section for the production of 3914 band photons, k=INL/e, $A=\Omega T_r FQ\varepsilon$, Ω is the fractional solid angle subtended by the specified photometer, T_r is the transmission of the photometer optics excepting

the filter, F is the filter transmission, Q is the quantum efficiency of the PM tube and ε is the efficiency of the electronics. (See Figures 11 and 12 for details of optical detection.) The accidental counting rate is then

$$\dot{N}_A = 2\tau \quad (\dot{N}_H + \dot{N}_{DH})(\dot{N}_N + \dot{N}_{DN})$$

where $\dot{N}_D$ is the dark counting rate for the specified photometer. The associated noise is then

$$N = \sqrt{N_A} = \left[2\tau T[\dot{N}_N \dot{N}_H + (\dot{N}_{DH}\dot{N}_N + \dot{N}_{DN}\dot{N}_H) + \dot{N}_{DH}\dot{N}_{DN}]\right]^{\frac{1}{2}}.$$

The signal rate is approximately

$$\dot{N}_R = kA_1A_2P_e\left[\sigma_c(3p,B) + \sigma_c(3d,B)\right].$$

Letting

$$\sigma_c \equiv \sigma_c(3p,B) + \sigma_c(3d,B)$$

gives

$$N_R = kA_1A_2P_e\sigma_c T.$$

The STN ratio is then

$$STN = \frac{A_1A_2\sigma_c(P_e^2/\tau)^{\frac{1}{2}}\,T^{\frac{1}{2}}}{2^{\frac{1}{2}}\left[A_1A_2Q\sigma_{3914} + \frac{e}{INL}\left(A_2\sigma_{3914}\dot{N}_{DH} + A_1Q\dot{N}_{DN}\right) + \left(\frac{e}{INL}\right)^2 \dot{N}_{DH}\dot{N}_{DN}\right]^{\frac{1}{2}}}.$$

In the case that $\dot{N}_{DH} << \dot{N}_H$ and $\dot{N}_{DN} << \dot{N}_N$,

$$STN = \sigma_c\left(\frac{A_1A_2}{2Q\sigma_{3914}}\right)^{\frac{1}{2}}\left(\frac{P_e^2}{\tau}\right)^{\frac{1}{2}}T^{\frac{1}{2}}.$$

In this case, there is no dependence of STN upon I or N and the only dependence on L comes through the P_e factor.

As was mentioned in an earlier section, a STN ratio on the order of 30 would be practically impossible to obtain in this experiment. The reasoning for this becomes apparent if the size of the STN ratio is estimated. Using experimentally determined values of $A_1 = 1.5 \times 10^{-3}$, $A_2 = 2 \times 10^{-3}$, $Q \approx \sigma_\alpha = 2 \times 10^{-17}$ cm^2, $\sigma_{3914} = 10^{-16}$ cm^2, $\tau = 70$ nsec, $P_e = .33$, and $\sigma_c = 1.0 \times 10^{-18}$ cm^2 (see Chapter V, section c) in the simplified expression above for STN, it is found that the time required to obtain a given STN ratio is on the order of

$$T = (STN)^2 \, 10^3 \text{ sec.}$$

For a STN ratio of 10, the required integrating time would be on the order of 28 hours. To obtain a STN ratio of 30 would require an estimated integrating time of about 10 days.

h) Considerations to Maximize STN

Inspection of the simplified expression for STN shows that the STN ratio will be maximized under the following experimental conditions:

1) long integrating time T,

2) choice of τ such that P_e^2/τ is maximized,

3) large values of A_1, A_2.

A discussion of these points will now be made.

1) The choice of integrating time is influenced mainly by the practical limitations on the time available for the

experiment. The total integrating time per data point finally used here averaged about 6 hours.

2) Figure 6 is a plot of P_e^2/τ as a function of τ for several values of L/v. In all cases, the maximum occurs in the neighborhood of τ=70 nsec and P_e^2/τ varies slowly in this region. This is contrary to the usual condition in nuclear coincidence experiments where the STN ratio is increased as τ is decreased. The difference clearly arises from the fact that in most nuclear applications the lifetimes involved are so small that the maximum signal to noise occurs at values of τ less than can be achieved with present electronics whereas in the present application, the lifetimes are long enough to give a maximum signal to noise at larger values of τ. It is interesting to note that this maximum occurs at approximately the lifetime of the excited N_2^+ state (the longer lived of the excited particles).

3) The A factors depend on detection geometry, filter transmissions, and the quantum efficiency of the PM tubes.

The optical detection apparatus consists of lenses that project an image of the beam onto the photosurfaces of the PM tubes (Figure 12). The optimization in the STN ratio is effected by determining the value of the object and image distances and the length of beam viewed that optimize the product ΩP_e, where Ω is the fractional solid angle subtended by the lens. For a circular lens of radius a looking at a point on the optical axis a distance d away,

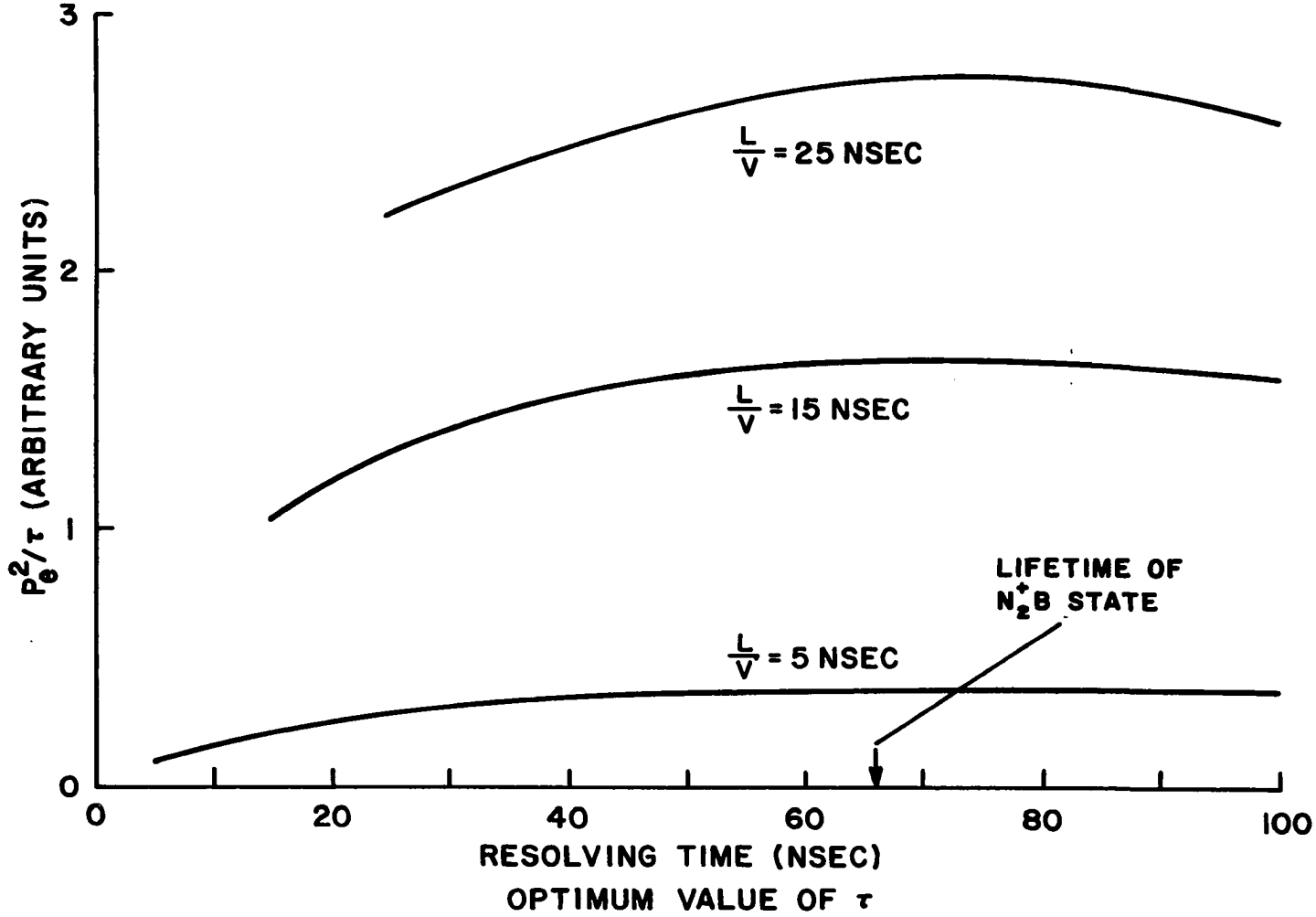

OPTIMUM VALUE OF τ

FIGURE 6

$$\Omega = \frac{1}{2}\left[1 - \frac{d}{(a^2+d^2)^{\frac{1}{2}}}\right] .$$

Using the simple lens formula, and the fact that the image size should be the same size as the photocathode, it can be shown that

$$d = f\left(1 + \frac{1}{M}\right),\ s = f\,(1 + M),\ \text{and}\ M = y/L$$

where d is the object distance, s is the image distance, f is the focal length of the lens, M is the magnification, y is the diameter of the photocathode and L is the object length--that is, the length of beam observed. Then, knowing f, a, and y, Ω can be calculated as a function of L. Using the above equation for Ω, and plotting ΩP_e as a function of L (Figure 7) it is seen that a value of 1 or 2 cm gives an optimization for most velocities. This corresponds roughly to a value of M=2, d=7 cm, and s=14 cm when f=4.6 cm, a=3.35 cm, and y=3.8 cm. The lens itself was chosen because of its high diameter to focal length ratio thereby giving a large value for Ω.

Since, using the detection geometry already described, light strikes the filter at angles as large as 20°, interference filters having fairly wide transmission bands with flat tops were used. This has the effect of keeping the transmission at the wavelengths of interest fairly constant (and as high as possible) with angle of incidence (see Figures 8 and 9). The objection to such wide filters is that unwanted emissions may contribute to the signal. In the case of the 3914 band photon

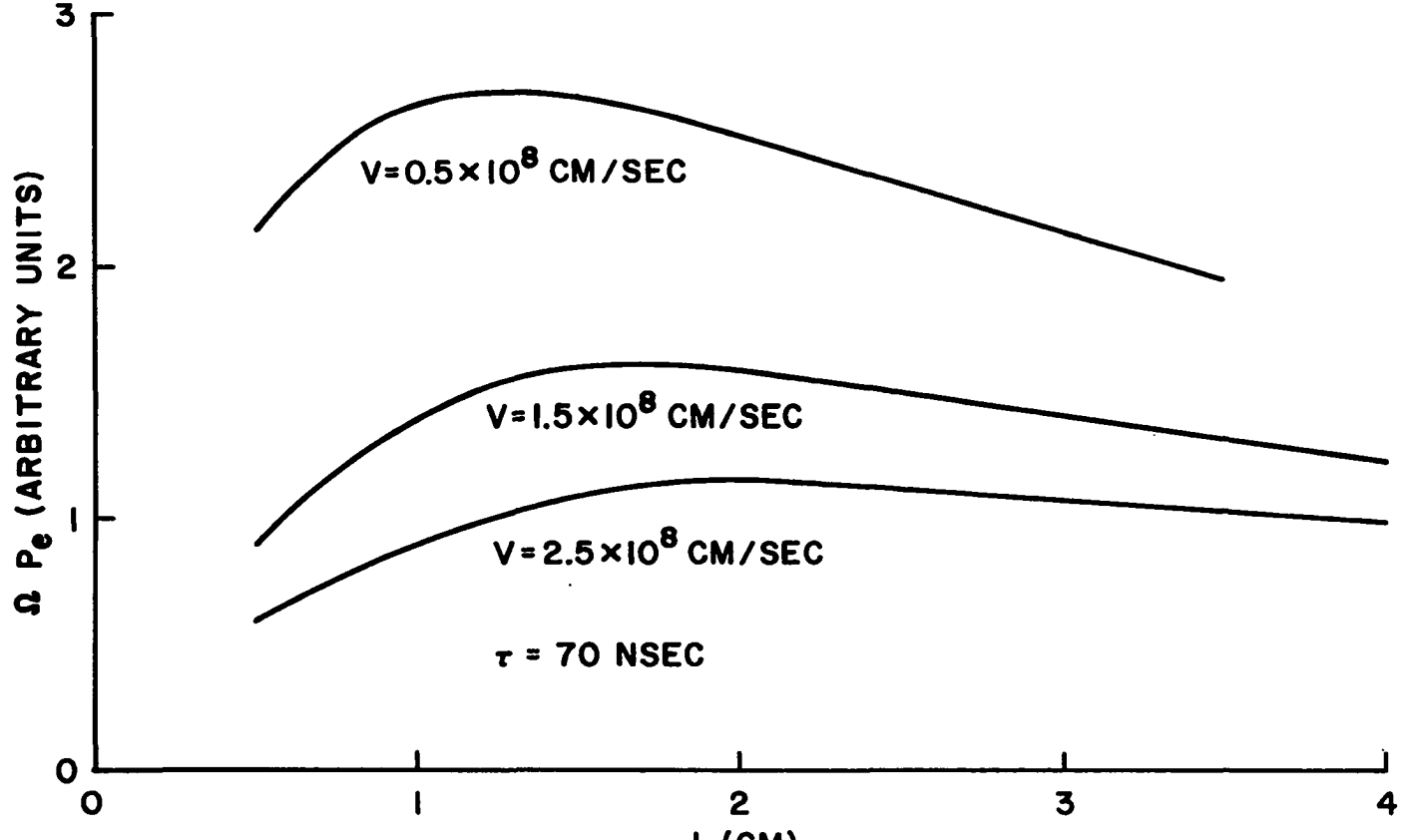

OPTIMIZATION OF GEOMETRY

FIGURE 7

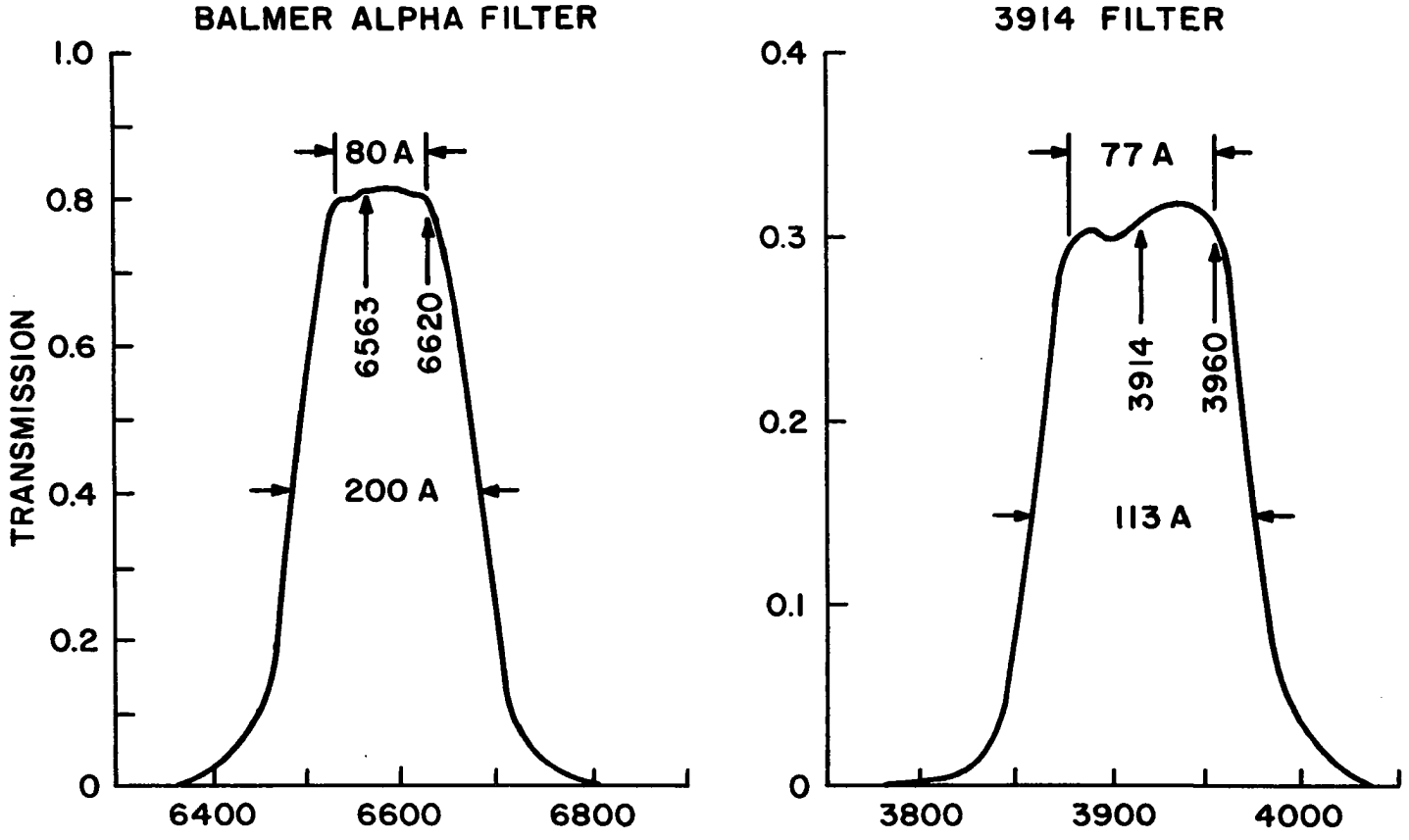

FILTER TRANSMISSION CURVES

FIGURE 8

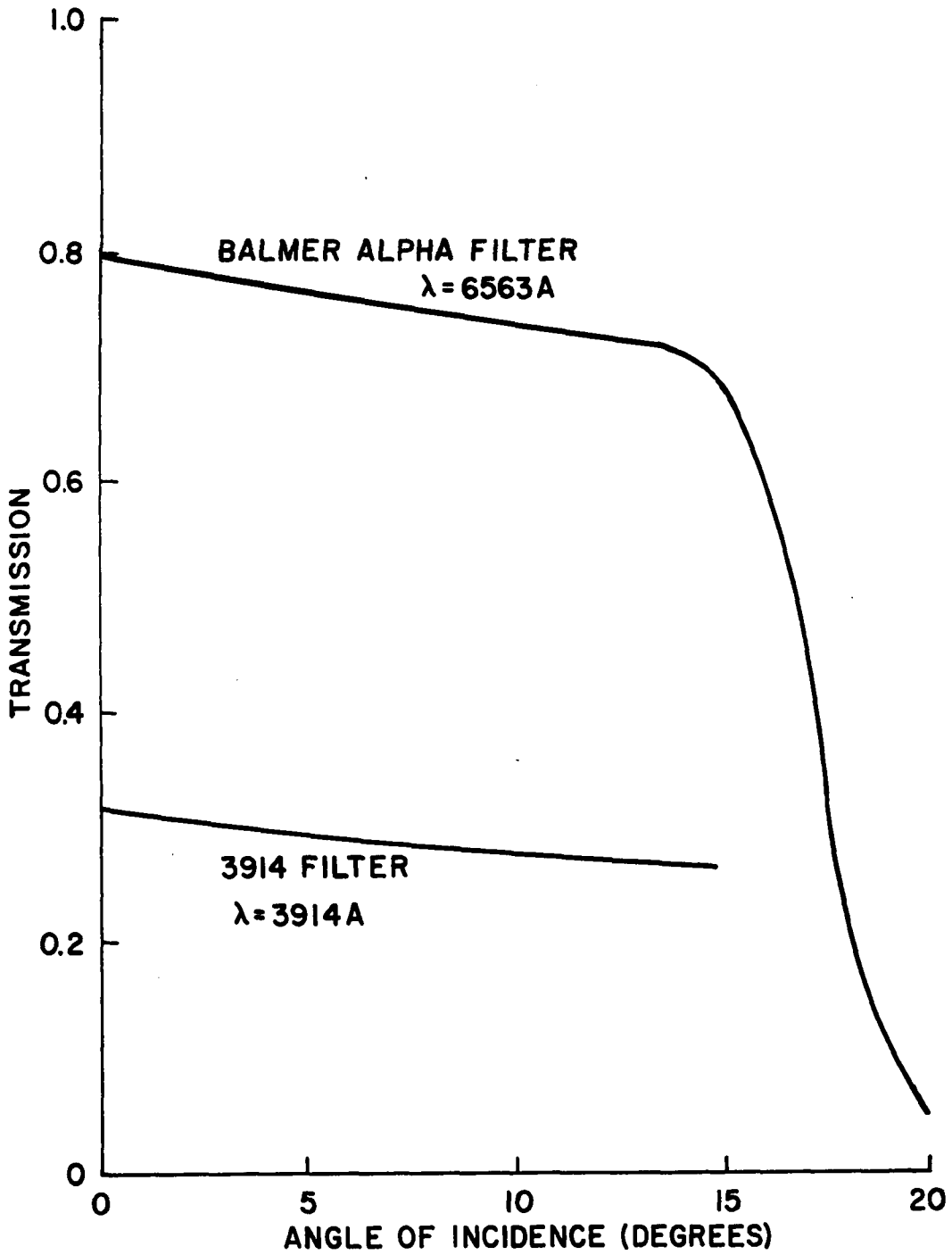

TRANSMISSION OF FILTERS WITH ANGLE OF INCIDENCE

FIGURE 9

detector, the only nearby band that might contribute would be the 3885 band of the 1st negative system of N_2^+, but the band ratio of 3914 to 3885 measured by Sheridan and Clark (1965) and others was found to be about 20 and shows that the 3885 band contribution may be neglected. A spectroscopic scan of the region around 3914A by Dahlberg et al. (1967) further confirms that the 3914A emission is by far the most prominent spectral feature. In the case of the Balmer alpha photon detector, the only close band emission is the N_2 1st positive emission whose excitation, however, is forbidden in proton impact. Also, pressures used in this experiment ($\sim 10^{-4}$ torr) are low enough so that negligible N_2 1st positive emissions are produced by second order processes (see Carleton, 1957). Observations by Carleton in this region further show that the Balmer alpha line is the strongest emission feature in this region.

Another point to mention concerning unwanted emissions is that any hydrogen emissions detected by the 3914 band photon detector can only add to the noise and cannot enhance the real coincidence signal. The same holds true for nitrogen (N_2, N_2^+, N, or N^+) emissions detected by the Balmer alpha detector.

The A factors are further increased if the photomultiplier tubes selected have photocathodes of high quantum efficiency at their respective wavelengths. The RCA 7265 PM tube used here has an S-20 surface with a quantum efficiency of about 4% at 6563A and about 20% at 3914A.

i) Beam Current and Pressure

In the approximate equation for the STN ratio given in the preceding section, there is no dependence on pressure or beam current. However, other considerations place limitations on the values of these variables. Usually in atomic collision cross section measurements, the pressure must be kept low enough so that one is assured of seeing only first order collision processes and so that collisional quenching of excited emitters is negligible. The requirement with respect to first order collisions may be relaxed somewhat in this type of experiment since second order processes leading to an error in signal are discriminated against by the time correlation. However, these second order processes may contribute significantly to the accidental counting rate (that is, to the noise). Short of a very detailed analysis, this condition can only be checked experimentally, and the best way to avoid trouble is to operate in the pressure range where previous experience has shown the single-collision, non-quenching region to be.

A limitation on the magnitude of beam current is given by the effects of Stark mixing of the n = 3 levels due to the electric field set up by the beam. (Stray electric fields are eliminated by the presence of grounded shields around the collision region.) The electric field magnitude at the edge of a beam with circular cross section and homogeneous charge density across the cross section is

$$E = \frac{I}{2vR\varepsilon_o}$$

where I is the beam current, v is the beam velocity, ε_o is the electric permittivity constant, and R is the radius of the beam. Using R = 2 mm

and $v = 0.5 \times 10^8$ cm/sec, the magnitude as a function of beam current in microamperes is

$$E = 0.6\ I \text{ volts/cm.}$$

The critical field strength for mixing of the $3P_{3/2}$ and $3D_{3/2}$ states is $E_c = 1.9$ volts/cm (Bethe and Salpeter, 1957). If it is required that the electric field magnitude caused by the beam be less than 1% of this value, then the beam current must be less than about .03 microamperes. This corresponds to the smallest velocity used and is a worst case situation.

One other limitation on the size of the beam current and pressure is that neither should be so large that the counting rate of the individual detectors exceeds the counting capacity of the detection electronics. The limiting feature here is the longest dead time, τ_D, of any component in the detection system. In this case, τ_D is about 2 microsec (for the pulse height analyzer). If the fraction of pulses lost due to the dead time (which is $\dot{N}\tau_D$ where $\dot{N}$ is the input counting rate to the pulse height analyzer) should not be greater than about 10%, then $\dot{N}$ should be less than about 5×10^4 sec^{-1}. The counting rate could be decreased by decreasing ϵ but this decreases the STN ratio since the A factors are proportionally decreased.

CHAPTER III

APPARATUS

a) Ion Beam System

The ion beam system used here is described in detail by Murray (1968). In brief, protons are produced in an Oak Ridge type hydrogen RF discharge (see Figure 10), extracted, accelerated, focused, magnetically mass analyzed, and finally collimated at the entrance to the collision chamber. The particle flux associated with this collimated proton beam is measured at the far end of the collision chamber with a Faraday cup. The limits of proton beam energy are about 2 and 30 keV and the beam energy resolution is at least 200 eV.

Calibration of the beam energy is accomplished by comparing the mass analyzer magnet current control setting with the energy deduced from a retarding potential measurement made at the position of the Faraday cup. This procedure is described in detail in the above referenced thesis by Murray (1968).

b) Collision Chamber

The entire collision chamber is shown in Figure 11 and the details of the optical detection in Figure 12. The light emitted from the collision region at a distance of 17.8 cm into the collision chamber is collected by plano-convex lenses of small f number (f=.70) and the image of this region is focused onto the photocathodes of RCA 7265 PM tubes after passage through quartz vacuum windows and interference filters. The beam diameter at this point is about .5 cm. The length of beam viewed is determined by

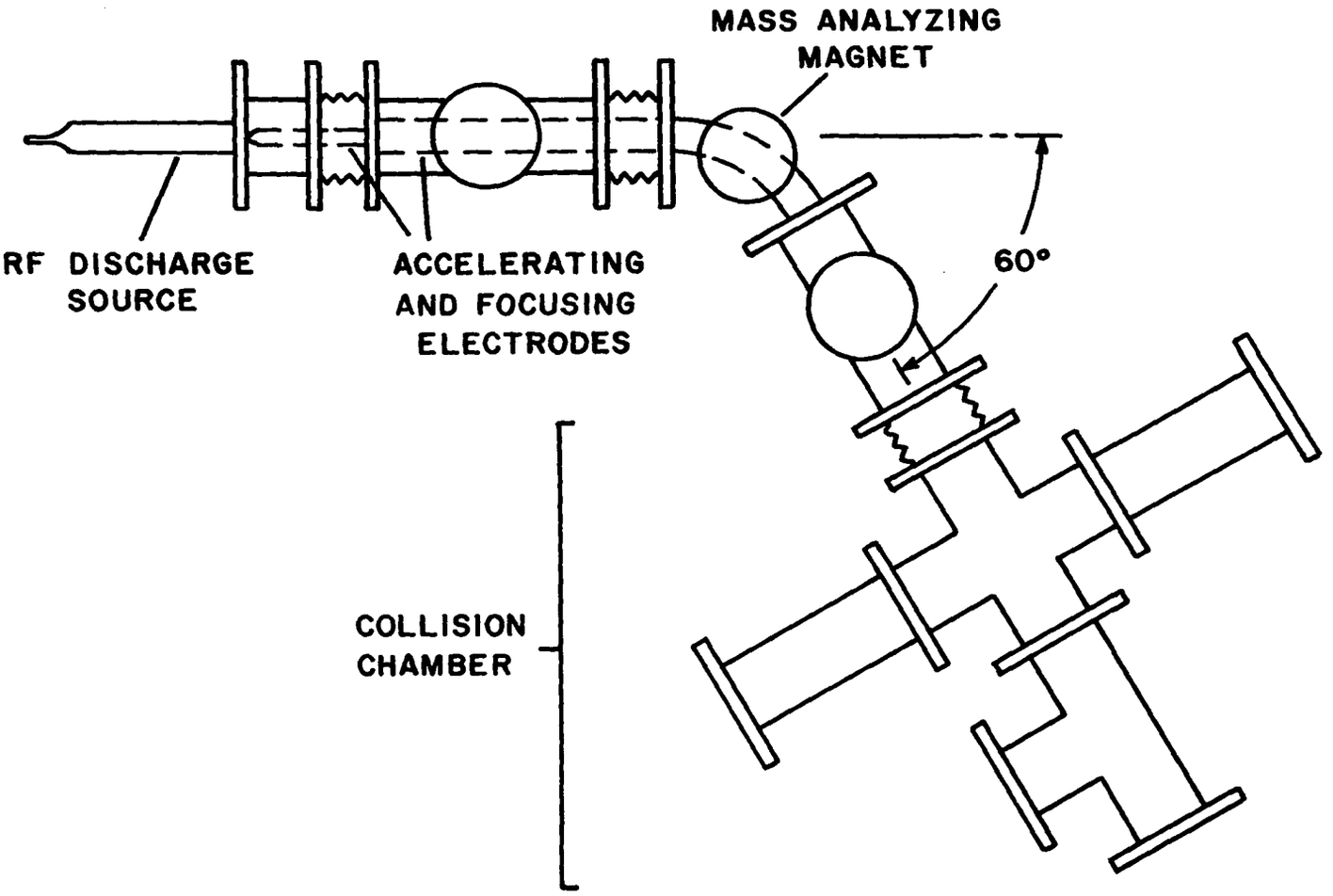

OVERALL APPARATUS
FIGURE 10

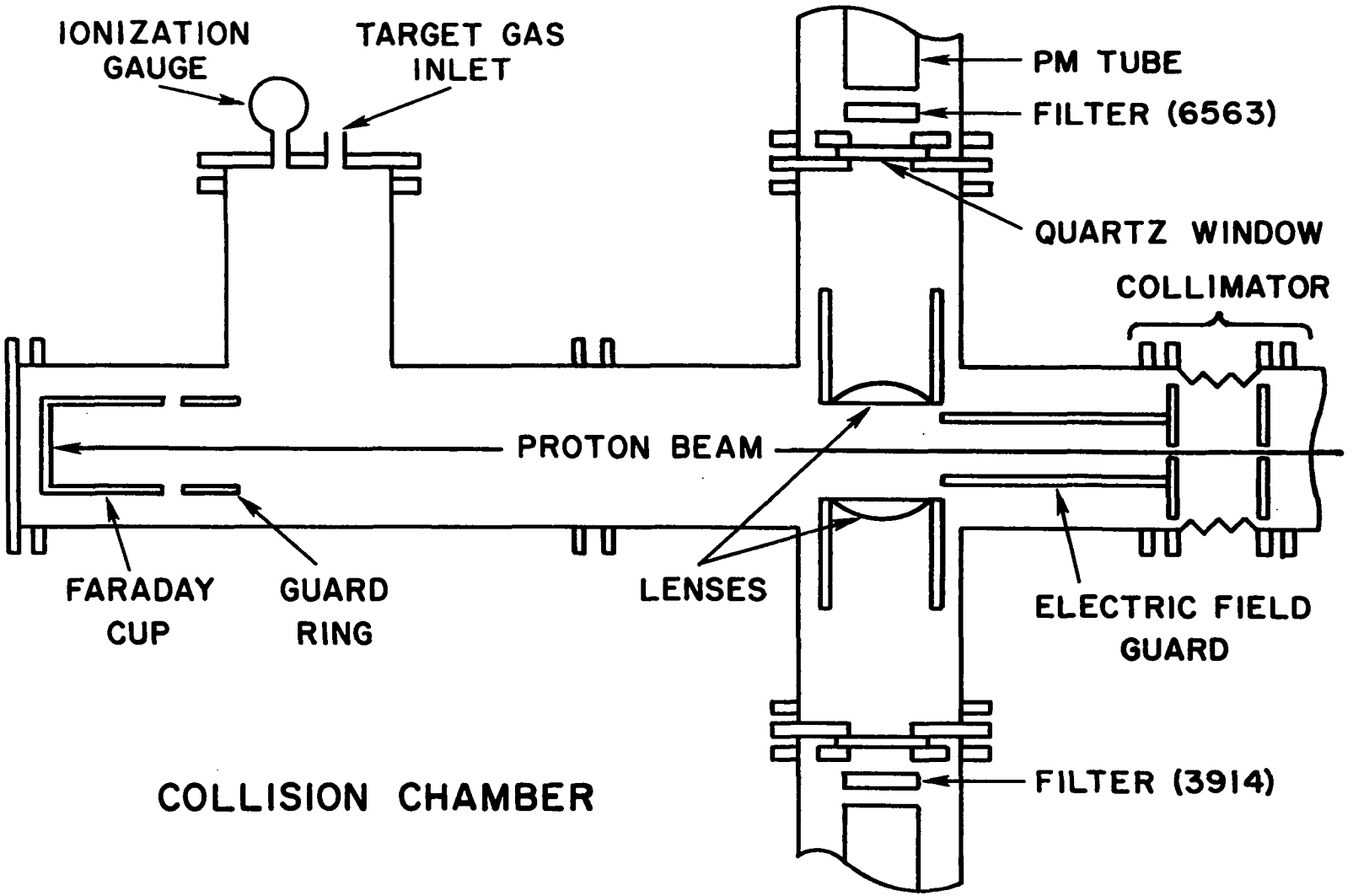

FIGURE II

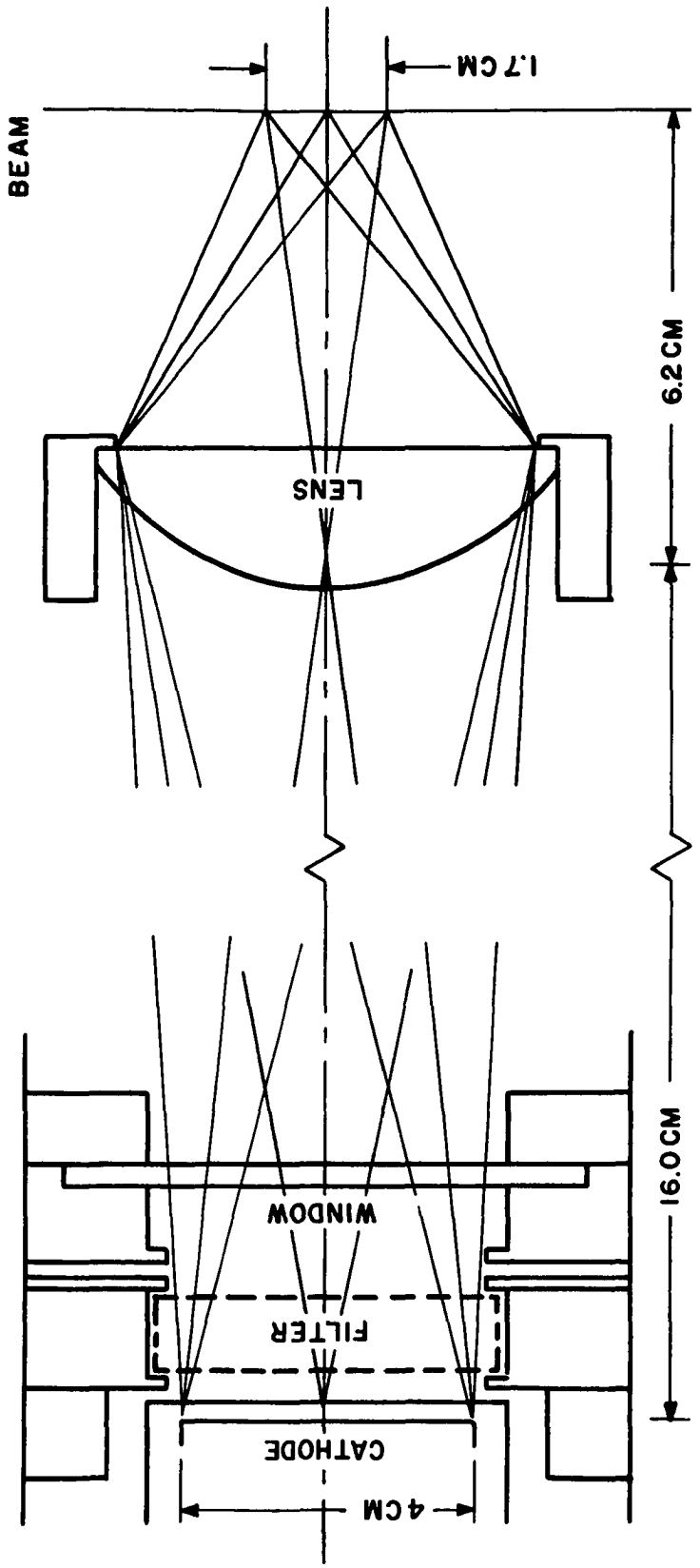

OPTICAL DETECTION GEOMETRY

FIGURE 12

the width of the photocathodes and the effective magnification of the lenses. The two lenses are individually adjusted in position to give the same magnification and to insure that each photometer is looking at the same length of beam at the same position on the beam. The object in this procedure is a taut wire stretched along the position of the beam path. A particular section of the wire is defined by a cardboard slit of about 1.2 cm width and the image of this slit is focused on screens placed at the positions of the photocathodes. In this manner, it is determined that the beam length which is viewed by both photometers is 1.7 ± .2 cm.

A grounded aluminum cylinder is placed along the entire length of the collision chamber from the entrance to the viewing region to guard against stray electric fields which could possibly cause level mixing in the hydrogen states (see section i, Chapter II).

The target gas is introduced into the collision chamber through a variable leak. It has been found from previous measurements that liquid nitrogen trapping in the inlet gas line is not necessary if the collision chamber and inlet line are well flushed with the target gas. The nitrogen target gas used here is of the prepurified grade. The collision chamber is prepared by first evacuating to a pressure of 3×10^{-6} torr. Nitrogen gas is then allowed to flow through the system at a high pressure (about .2 torr) for about an hour. The chamber is then again evacuated to 3×10^{-6} after which the gas pressure is adjusted with the variable leak to a final pressure of about 10^{-4} torr and the system allowed to sit for at least 12 hours before actual pressure measurements are made. After the 12-hour stabilization time, the target gas pressure

remains constant to within 2% over periods as long as two weeks although pressure measurements are made considerably more often. All pressure measurements are made with an ionization gauge according to the procedure outlined by Murray (1968).

c) Beam Measurement

The beam current is measured with a Faraday cup equipped with a negatively biased guard ring to help prevent secondary electrons formed by the impinging beam from leaving the cup. The bias voltage is about 30 volts for all beam energies used. The beam current thus collected is integrated by means of a commercial integrator over the signal detection time to give directly the charge collected during that time. The entrance to the Faraday cup is located 45.3 cm from the point of optical observation. A correction for charge exchange degradation of the proton beam over this length is made in the data reduction to give the proton charge which actually passes through the viewing region.

d) Signal Detection

The signal detection system consists of two detector channels, a switching module, a coincidence detector, and two scalers (see Figure 13).

The detection channels (one for detection of Balmer alpha photons and one for detection of 3914 band photons) each consist of a photometer (PM tube plus interference filter), a preamplifier, a double delay line amplifier (DDL) and a pulse height analyzer (PHA). Each detection channel is a single photon detector since the average time between anode pulses is much longer than the anode rise time of the PM tube. An estimate of

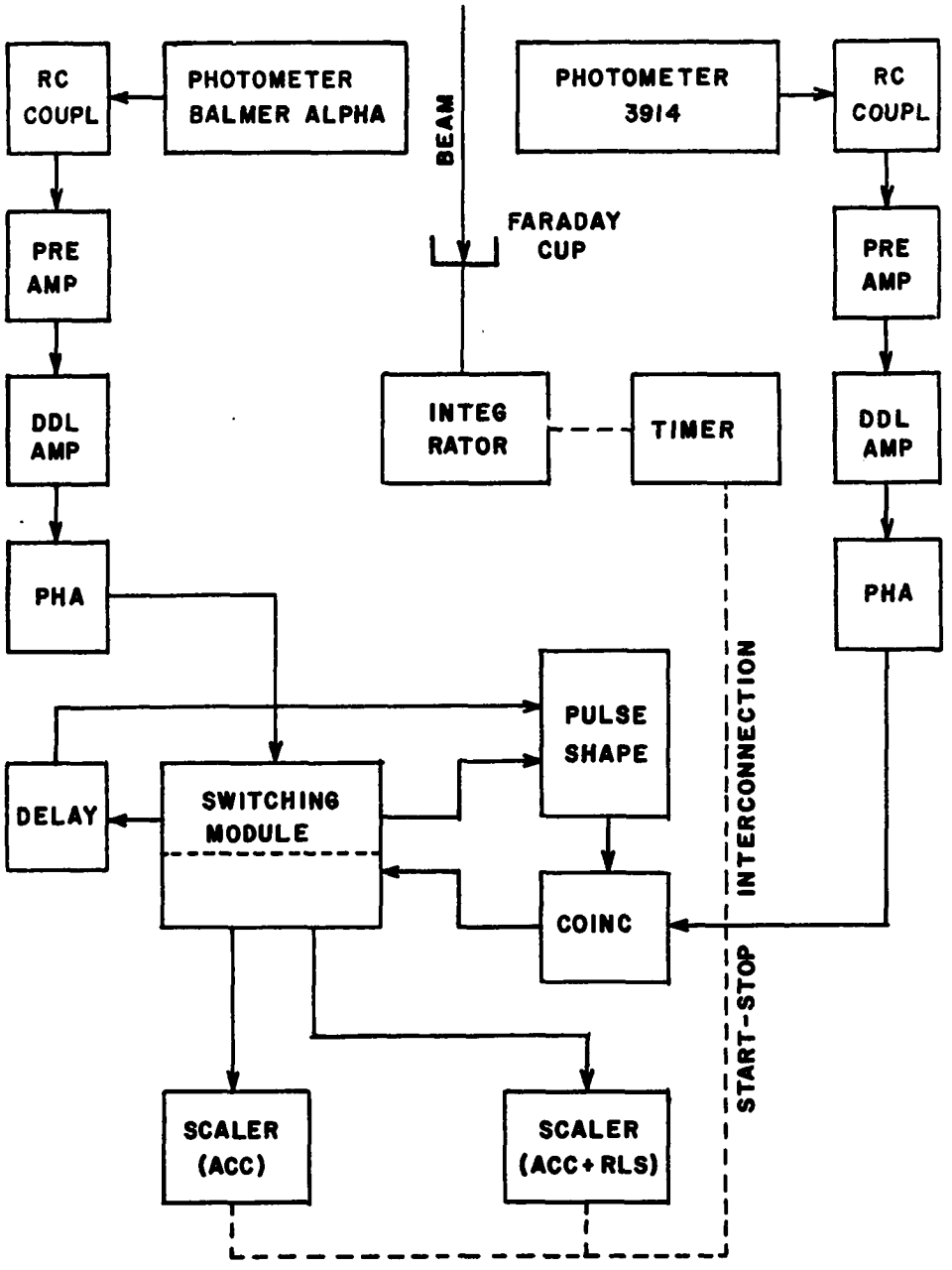

SIGNAL DETECTION ELECTRONICS

FIGURE 13

the maximum detection rate under experimental conditions is $5 \times 10^{7} sec^{-1}$. This gives an average time between anode pulses of 20 nsec whereas the anode rise time of the RCA 7265 PM tube is specified at 3 nsec. The current pulses from the PM tube (which then represent the arrival of individual photons at the cathode or represent dark counts) are passed through a 2.2 MΩ resistor to ground and the resulting potential used to charge a 100 pf capacitor. The potential across this capacitor is then used as an input voltage pulse to the preamplifier. The preamplifier output pulse is carried to the DDL amplifier by 50 Ω impedance coaxial cable. (Interconnections between components throughout the entire signal detection apparatus are made with 50 Ω coaxial cable.) The resulting wave form at the input to the DDL amplifier has a risetime of about 30 nsec and a decay time of about 150 μsec. The DDL amplifier is operated in the cross-over mode and the resulting zero reference cross-over point between the positive and negative phase of the output pulse used to trigger the following PHA. The DDL amplifier has a linear gain up to the point where the output pulses are 10 volts peak-to-peak. Thereafter, the output pulses are clipped at 10 volts peak-to-peak. The DDL amplifier gain setting is adjusted fairly low so that a clean, undistorted output pulse results. The low gain is compensated for by operating the PM tubes at fairly high voltages (about 2300 volts for each tube). The PHA threshold is set to eliminate only the very smallest of DDL amplifier output pulses and the PHA window is set to just eliminate the clipped pulses of the DDL amplifier. This procedure helps to insure that possible large or small signals from external sources (such as the RF discharge of the proton source) do not

contribute to the counting rates. The PHA sensitivity is then set just above the threshold value where all DDL output pulses allowed by these settings are detected. The output pulse of the PHA has a rise and fall time of about 10 nsec with a width of 200 nsec.

The output pulses from the PHA in the 3914 band photon detector are sent directly to one of the inputs of the coincidence detector. The output pulse from the Balmer alpha detection channel are sent to the input of the switching module.

The switching module is essentially a DPDT (double-pole, double-throw) electronic switch formed by driving two SPDT (single-pole, double-throw) switches in phase (see Figure 14). The SPDT switches are formed by combining two ON-OFF switches in parallel. These ON-OFF switches are driven by a 12.5 Hz, 4 volt square wave which is derived from a 100 Hz thermostatically controlled crystal oscillator and a three-stage, bistable multivibrator, frequency divider (see Figure 15 for divider schematic). The ON-OFF switches are constructed so that they are in their conducting state (ON) when the positive phase of the square wave is applied to the switch and in their nonconducting state (OFF) when the zero phase is applied (see switch schematic, Figure 16). One side of each SPDT switch is driven with the normal phase of this wave form while the other side is driven with the inverted phase thus giving the SPDT effect (see Figure 17 for inverter schematic). The symmetry of the square wave form is better than 1 part in 10^6. The switching time between the conducting and nonconducting states of the ON-OFF switches is less than 100 nsec (which is very small compared to the 40 msec half-period of the switching frequency). The fraction of real coincidences lost due to their occurrence during the switching

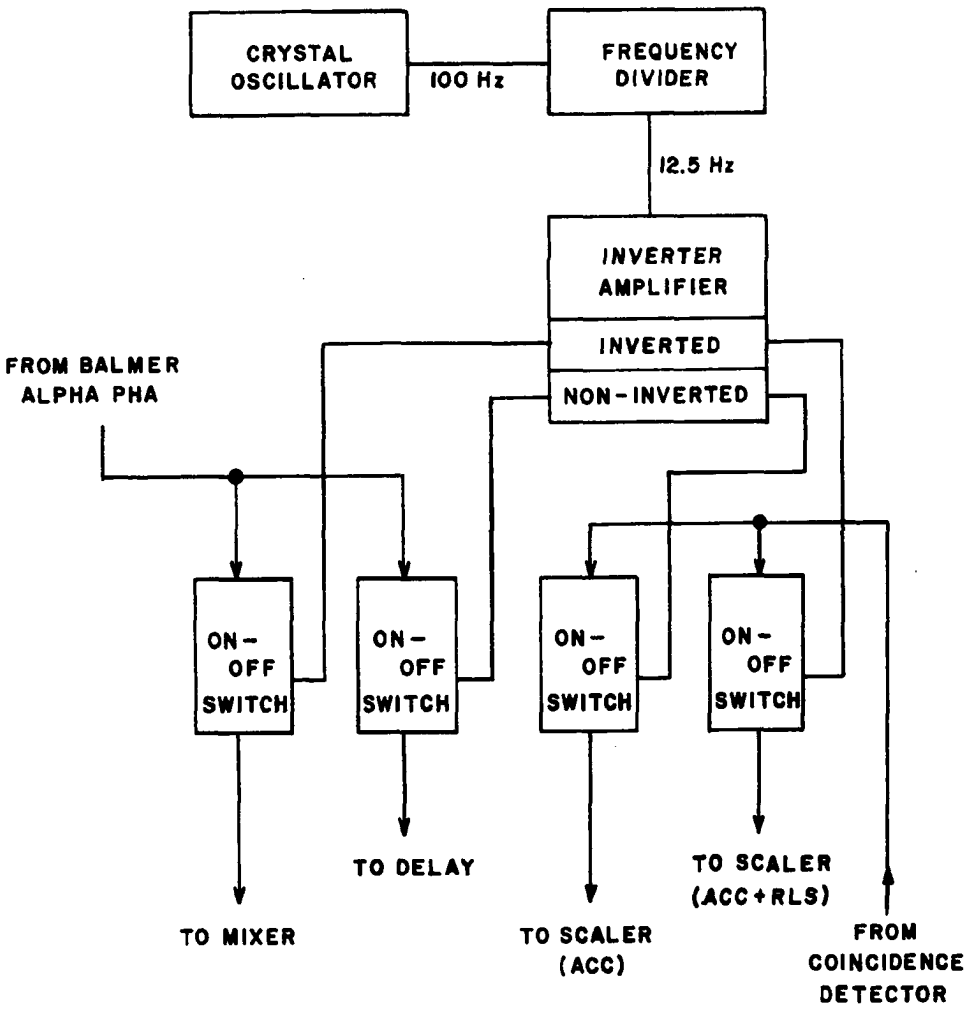

SWITCHING MODULE BLOCK DIAGRAM

FIGURE 14

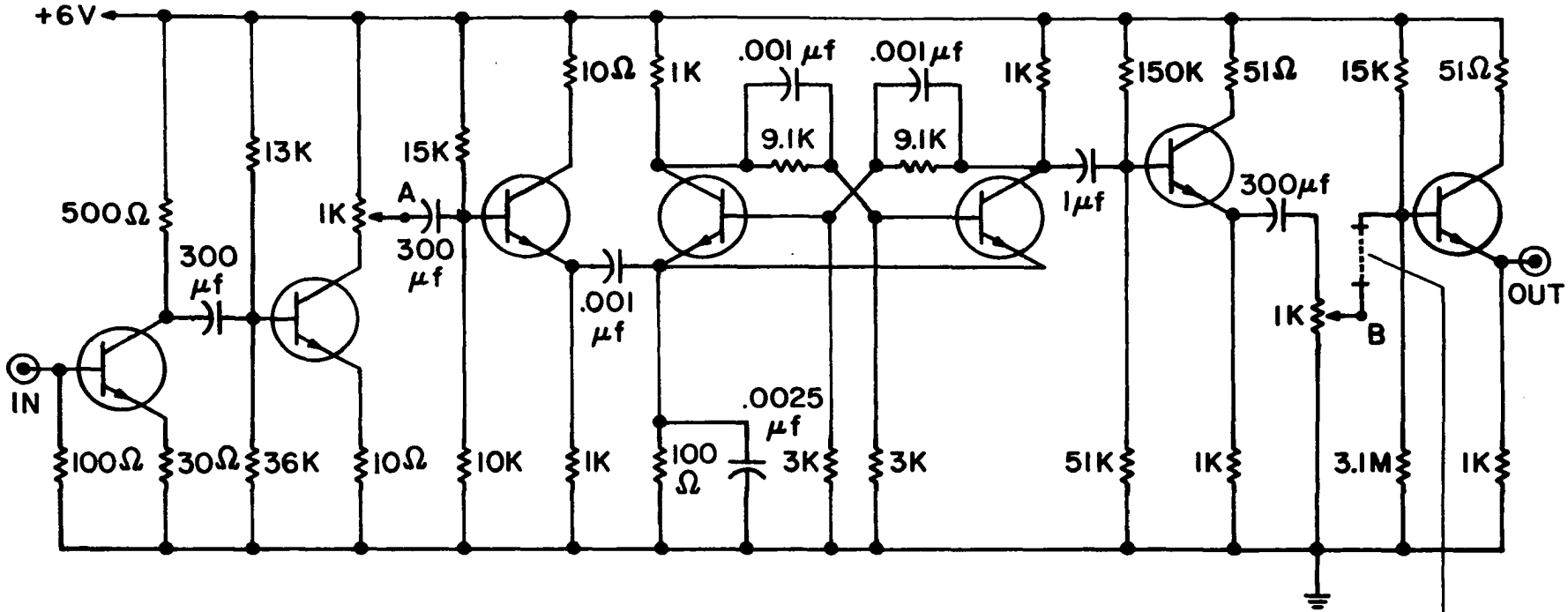

FREQUENCY DIVIDER

FIGURE 15

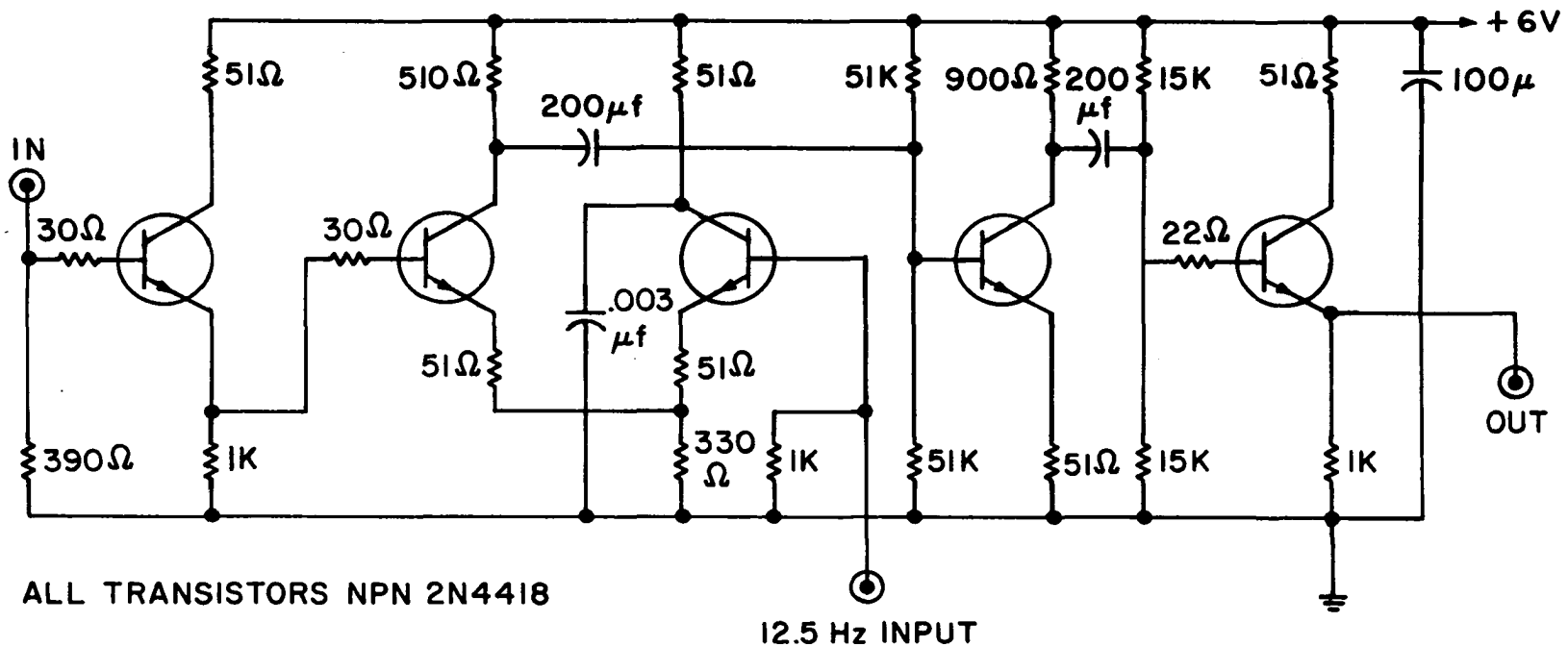

SWITCH SCHEMATIC

FIGURE 16

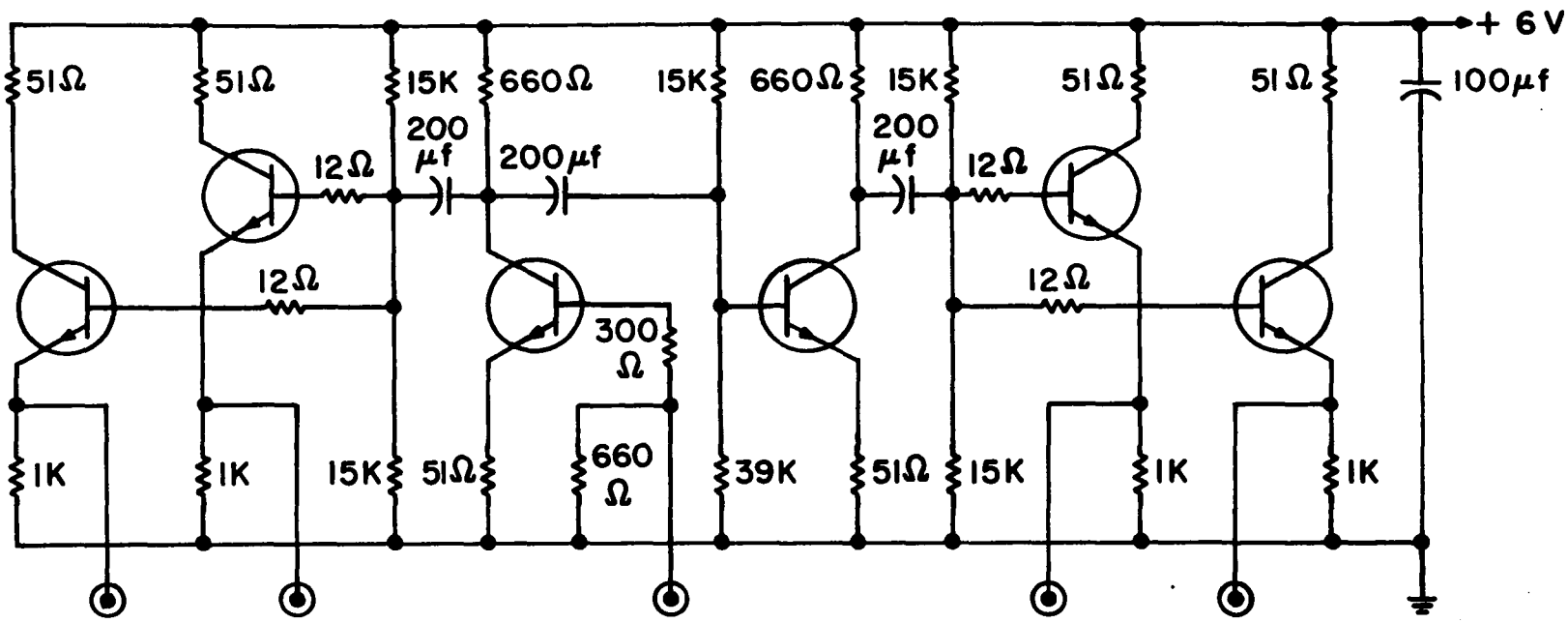

INVERTER AMPLIFIER

FIGURE 17

time is approximately the ratio of these two time periods and is hence negligible.

Pulses from the Balmer alpha photon detection channel are led to the input of one of the SPDT switches where they are alternately passed directly to a pulse shaping stage or through a 200 nsec delay and then to the pulse shaping stage. The output pulses from the pulse shaping stage are led to the second input of the coincidence detector. The pulse shaping stage insures that pulses arriving at the coincidence module during the delayed and undelayed phase are the same shape and size. This precaution is taken so that no systematic error arises due to small differences in coincidence detector input wave forms during the two phases.

The output pulses from the coincidence detector due to coincidences between pulses arriving from the 3914 band photon detection channel and the pulse shaping stage are similarly routed with the other SPDT switch to one or the other of the two scalers. Since the two SPDT switches which form the DPDT switch are exactly in phase, the pulses counted on one scaler are coincidences between the 3914 band photon detector pulses and undelayed pulses from the pulse shaping stage and hence constitute accidental coincidences plus real coincidences (N_A+N_R) (see Chapter I) while the pulses counted on the other scaler are coincidences between the 3914 band photon detector pulses and the delayed pulses from the pulse shaping stage and hence constitute accidental coincidences (N_A) only.

The purpose of the switching module is to average out fluctuations and drifts that may occur in the beam current, coincidence resolving time, and detector sensitivities over the relatively long integrating times used (about 1 hour).

To insure that the time paths from the time of emission of the two photons to the arrival of the resulting pulses at the coincidence detector are equal, the inputs to the coincidence detector are monitored with high impedence probes and a fast dual trace oscilloscope triggered by one of the inputs while both detection channels are connected to the output of one photometer. The variable delays provided on the PHA's are then varied to cause the two wave forms (one from the 3914 channel and the other from the pulse shaper during the undelayed phase) to coincide. Equalization to better than 2 nsec can be achieved in this manner. The jitter of the system is also observed with this display by noting how much the leading edge of the non-triggering wave form is spread out around the leading edge of the stable triggering wave form. The jitter is observed to have about a 5 nsec half width.

Since the two detection channels are connected to the same photomultiplier, the above procedure does not account for transit time differences between the two PM tubes, nor does it account for additional jitter caused by transit time variations in the PM tubes. However, the transit times for the RCA 7265 PM tubes at the voltages used here are characteristically only about 3 nsec so that only a small error can result from their exclusion. A more accurate method of making these measurements and adjustments would be to use a pulsed light source having very fast rise times and continuous emissions near 3914A and 6563A in the region of the collision volume and leaving each channel connected to its own PM tube.

e) System Checks

Several checks are made on the signal detection system to insure that it is working properly and does not introduce appreciable systematic errors in the signal data. The first of these checks is simply to monitor the input and output pulses of the various electronic components with an oscilloscope to verify that the signal pulses are clean, undistorted and are of sufficient voltage to drive the subsequent components correctly.

The system is checked for coincidence detection efficiency by connecting a mercury pulser of known frequency (about 30 Hz) to the input of both preamplifiers and noting that the "accidentals plus reals" scaler counts the correct number of pulses whereas the "accidentals" scaler counts only the number of pulses that result from "split pulses." This effect is due to the arrival of a pulse at the input of the switching module at such a time that the first part of the pulse is routed to one scaler while the second part of the pulse is routed to the other scaler. This effect is very small and is of the order τ_w/τ_s where τ_w is the pulse width (200 nsec) and τ_s is the switching half-period (40 msec). It is also verified that when pulses are allowed to enter only one input of the coincidence detector, no output pulses occur.

Another measurement made when only real coincidence pulses are present at the inputs to the preamplifiers is the cable curve of the system. For this measurement, a fixed delay of 100 nsec is inserted into one of the detection channels, a variable delay of 10 nsec to 300 nsec inserted into the other channel, and the coincidence counting rate, $\dot{N}_C$, measured as a function of the variable delay as the delay is changed in 1 nsec steps. The counting rate is either one of the channels, $\dot{N}_T$, is

used as a monitor. The resulting plot of $\dot{N}_C/\dot{N}_T$ is shown in Figure 18 along with the curve resulting when a similar measurement is made with the coincidence detector alone. The spreading out of the system cable curve at the edges of the coincidence detector cable curve is due to the effect of jitter as discussed in Chapter II. The amount of spreading is seen to be about 7 nsec which is in good agreement with the 5 nsec value observed with the oscilloscope display (section d, this chapter). The 2τ half-width of the system cable curve is used as the definition of the resolving time of the system.

In addition to detecting all coincidences that should be detected, one must insure that when no real signal is present (only accidental counts), no real signal is detected. For this check, the two photometers are illuminated with light from independent sources whose intensities are adjusted so that the counting rates approximate experimental conditions (see next chapter for typical experimental values). Since the two lights are independent, there is no real time correlation between pulses originating at the photomultipliers and hence there can be no signal. The apparent signal resulting from an average of 11 data points taken over a total integrating time of 5½ hours is 27 with a standard deviation of the mean of 169 indicating that within the expected random fluctuations (again see next chapter) no signal is observed.

f) Start-Stop Interconnection

The beam current integrator and the scalers recording the coincidence detector output pulses are interconnected with a mechanical timer so that beam detection and signal detection may be started and stopped simultaneously.

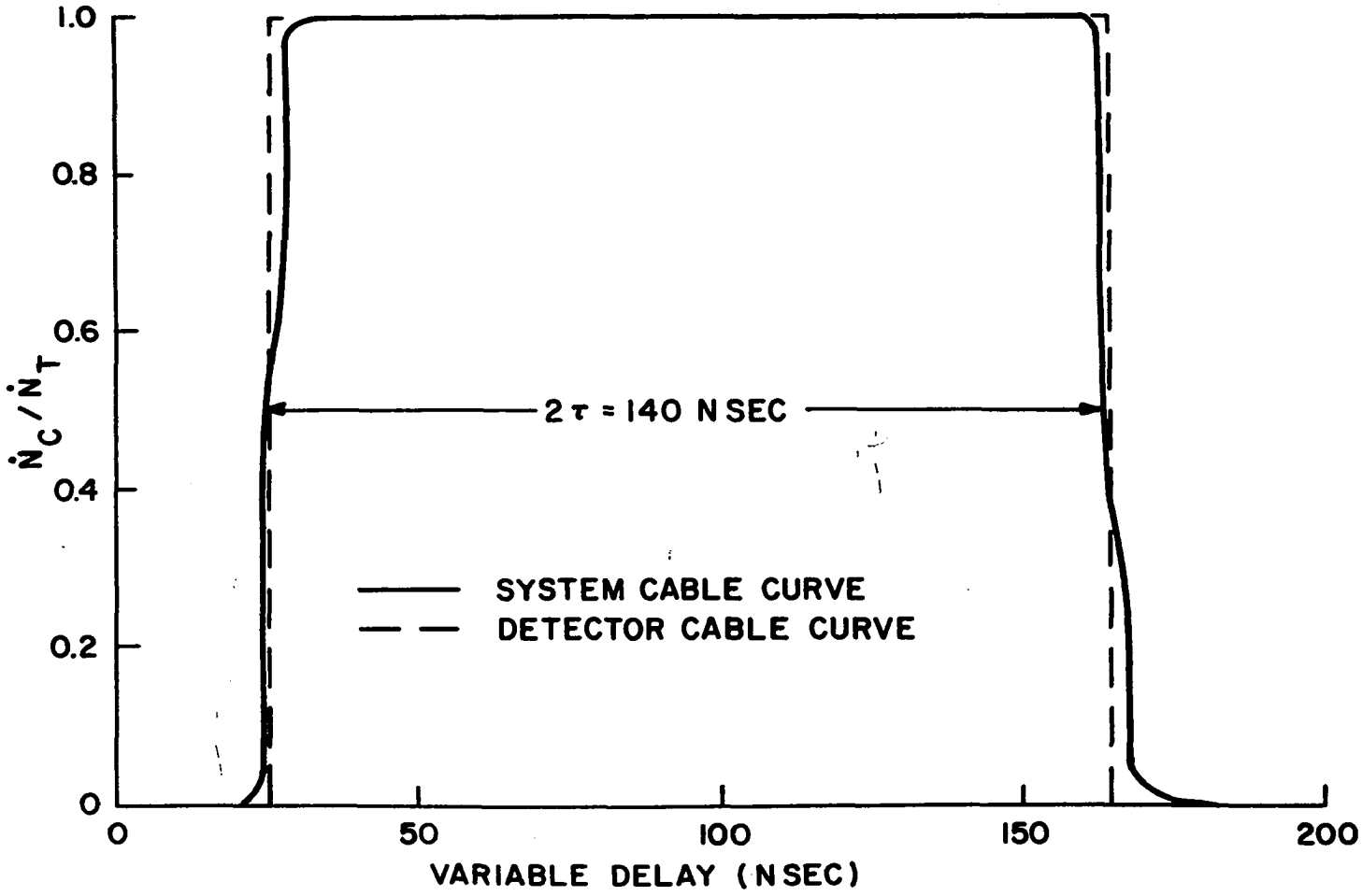

TYPICAL CABLE CURVES

FIGURE 18

The system is started manually and is stopped automatically either when a preset time has elapsed or a preset amount of beam charge has been collected.

CHAPTER IV

DATA REDUCTION

a) Data Taking Procedure

Data are taken using the detection arrangement shown in Figure 13. The number of counts recorded in time T by one scaler (ACC+RLS) is N_A+N_R and the number recorded by the other (ACC) is N_A. The signal, N_R, is obtained simply by subtracting the reading N_A from the reading N_A+N_R. This signal, together with a measurement of the beam charge, C, collected during the same time T is sufficient to determine the ratio of real coincidence counts to proton charge collected (counts/coulomb) at a particular proton velocity and target gas pressure. In the actual data taking procedure, the integrating time T is not set to a particular value, but rather the value of C is preset and the beam current, I, adjusted to give a value of T in the neighborhood of 1 hour. Care is taken in the selection of beam current and pressure so that the counting rates of the individual channels do not exceed the capabilities of the detection channels.

For each set of coincidence signal measurements (typically from 6 to 8 values of N_R are determined in one day), a pressure measurement of the target gas is made and one set of additional measurements is made for use in data reduction. The latter involves the simultaneous measurement of the signal counts at each PHA (N_H and N_N) and the beam charge, C', collected in a time T'. (Background counts are subtracted from the N_H and N_H data.)

Typical values occurring during a data run at a proton velocity of 1.16×10^8 cm/sec (7.4 keV) are:

Target gas pressure $p = 1.1 \times 10^{-4}$ torr

$T \simeq 75$ minutes

$I \simeq 7 \times 10^{-9}$ amperes

$C = 1/2\ (3 \times 10^{-5}$ coulombs) -- The factor 1/2 accounts for the fact that, because of the switching method of detection, real coincidences are counted for only 1/2 the time period T.

$N_A \simeq N_A + N_R \simeq 2 \times 10^5$

$N_R \simeq 700$

$T' = 1$ minute

$C' \simeq 3 \times 10^{-7}$ coulombs

$N_H \simeq 3.6 \times 10^5$

$N_N \simeq 2.5 \times 10^6$.

b) Data Statistics

At a particular beam velocity, n determinations of N_R are made ($n \simeq 10$). The theoretical standard deviation for this set of data is approximately

$$SE = \sqrt{\frac{2}{n} \sum_i N_A^{(i)}}$$

if the distribution of N_R is a Poisson distribution. The factor of 2 arises because of the subtraction of N_A on one scaler from N_A+N_R on the other. These two numbers are independent since (because of the switching method of detection) they are collected during different time periods and the error in the subtraction must reflect the fact that both numbers have an associated random error. The experimental standard deviation for this data set is

$$S = \sqrt{\frac{1}{n} \sum_i (\bar{N}_R - N_R^{(i)})^2}\ .$$

In all cases, S $\simeq$ SE indicating acceptable statistics.

The value chosen to represent the random error in $\bar{N}_R$ in this experiment is the 70% confidence limit, E, given by

$$E = S_{max}(n-1)^{-\frac{1}{2}}t(n).$$

Here, S_{max} is the greater of S or SE and t(n) is derived from the "Student t distribution" and has values 1.10, 1.09, 1.09, 1.08, and 1.08 for n = 9, 10, 11, 12, and 13 (see for example, Hoel, 1962).

c) Linearity of Signal

The signal, as measured by the method of the preceding sections, is checked for linearity with beam current and pressure. The results are shown in Figure 19 and display acceptable linearity within expected random fluctuations. The linearity with beam current data are taken at a velocity of 1.35×10^8 cm/sec (9.5 keV), a pressure of 1.1×10^{-4} torr, and are corrected for electronics dead time loss. The linearity of pressure data are taken at a velocity of 1.07×10^8 cm/sec (6.0 keV), normalized to a total beam charge collected of 1.5×10^{-5} coulombs, and corrected for both charge exchange degradation of the beam and dead time loss. The point at zero on the linearity with beam current figure is obtained by turning the beam off and observing coincidences between dark counts only. This point is not especially meaningful in the linearity check, but provides further evidence that the apparatus is working correctly by giving no signal when no signal is present.

The single counting rates $\dot{N}_H$ and $\dot{N}_N$ also show linearity with beam current and pressure after the degradation and dead time loss corrections.

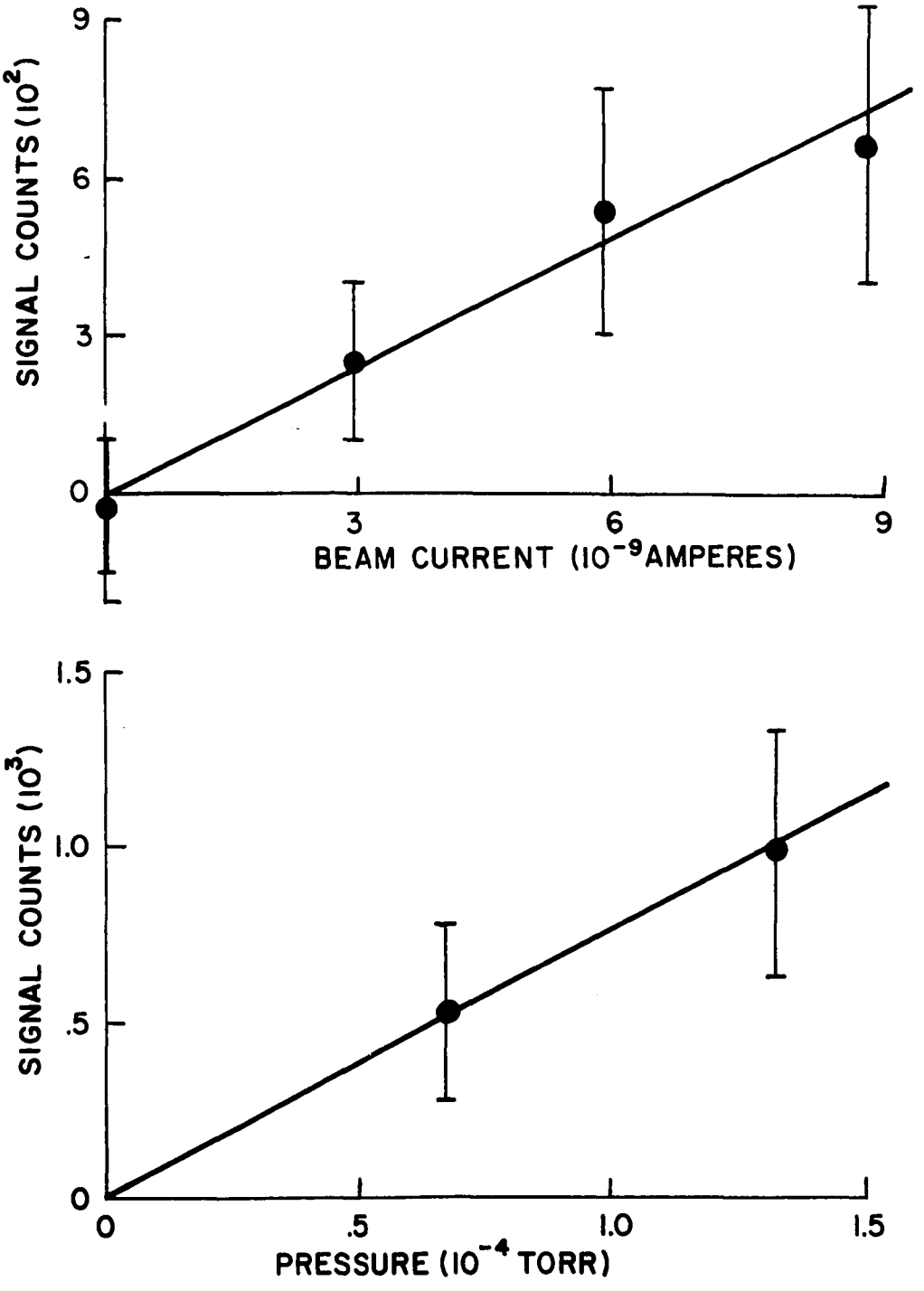

LINEARITY OF SIGNAL WITH BEAM CURRENT AND PRESSURE

FIGURE 19

The linearity of the various signals with beam current and pressure confirms that second order processes do not contribute significantly to the signal.

d) Data Reduction

The measured value of N_R is related to the emission cross sections by the approximate equation (see Chapter II, section e)

$$N_R = \frac{CNL}{e} A_1 A_2 P_e [\sigma_c(3p,B)+\sigma_c(3d,B)] \exp(N\sigma_{ce}d)$$

where C is one half the beam charge collected at the Faraday cup (as explained in section a of this chapter) and σ_{ce} is the total charge exchange cross section for proton impact on nitrogen. The exponential factor corrects for charge exchange degradation of the beam between the point of optical observation and the point at which the charge is collected (this distance d is 45.3 cm). Similarly, the individual detector counts in terms of total emission cross sections are

$$N_H = \frac{C'NL}{e} A_1 Q \exp(N\sigma_{ce}d)$$

and

$$N_N = \frac{C'NL}{e} A_2 \sigma_{3914} \exp(N\sigma_{ce}d).$$

σ_{3914} is the total cross section for the production of 3914 band emission whether by charge exchange or ionization, and Q is the "effective" cross section for the production of Balmer alpha photons at a distance of 17.8 cm into the collision chamber. (See Murray, 1968, for a discussion of beam equilibrium). More precisely,

$$Q = F_{3s}(z)\sigma_{3s} + F_{3p}(z)\sigma_{3p} + F_{3d}(z)\sigma_{3d}$$

where

$$F_{3m} = 1\text{-}\exp\,[-A(3m)z/v],$$

z is the distance of the observation region into the collision chamber, v is again the proton velocity, and A(3m) is the total transition probability from the 3m state. For z=17.8cm, both F_{3p} and F_{3d} are nearly 1 for all v in the region used so that

$$Q = F_{3s}\sigma_{3s} + (\sigma_{3p} + \sigma_{3d}).$$

Both Q and σ_{3914} are measured in separate experiments using the techniques described by Murray (1968) with the results shown in Figures 20 and 21 respectively.

The equations for N_R, N_H, and N_N yield

$$\sigma_c(3p,B) + \sigma_c(3d,B) = \frac{N_R}{N_H N_N}\,\frac{(C')^2}{C}\,\frac{NL}{e}\,\frac{\exp(N\sigma_{ce}d)}{P_e}\,Q\sigma_{3914}$$

as the final relation between the emission cross section and experimentally measured or known quantities. The value of G (see Chapter II, section e) may be obtained from this expression by multiplication with P_e.

e) Approximations and Errors in Data Reduction

The approximations and systematic errors associated with the experimental value for $\sigma_c(3p,B)+\sigma_c(3d,B)$ because of neglect of 3s → 2p and cascade contributions, evaluation of P_{3m} probabilities, averaging of P_{3p}

and P_{3d} to give P_e, beam length L, and errors introduced by the switching module have been discussed in previous chapters. The random error in N_R has been considered in section b of this chapter. Errors associated with fluctuations and drifts in τ, switching module symmetry, beam current, pressure, and detector sensitivities are automatically included in the evaluation of E. Since S and SE are always nearly equal, these effects are small. The percent random errors in N_H and N_N are given by expressions of the form $100(N)^{-1/2}$ which amount to less than 1% error since N_H and N_N are large. However, reproducibility of N_H and N_N measurements reveals an error of about 3%. Errors in C and C' are determined mainly by the accuracy of the current integrator and the effectiveness of secondary electron suppression at the Faraday cup. The combined error in C and C' due to these effects is estimated at less than 3%. The cross section σ_{ce} used here is an average of several published results (see next chapter, section d) with an estimated error of about 10%. The errors in Q and σ_{3914} measured in the present investigation are each estimated at 20%. (This includes random and systematic errors.)

The target gas particle density, N, is obtained from the measured gas pressure assuming the ideal gas law. The pressure is measured with an ionization gauge which is calibrated against a liquid nitrogen trapped McLeod gauge. The estimated error in the pressure calibration is 2% due to reproducibility and no more than 8% for the Ishii effect.

The value of τ used to compute P_e is determined by measuring the cable curve of the detection system as a whole (excluding PM tubes) as is described in the previous chapter (section e). The estimated error in τ, and hence also in P_e, is less than 2%.

The expression for $\sigma_c(3p,B)+\sigma_c(3d,B)$ is derived assuming that both the Balmer alpha and 3914 band radiation resulting from collisions of interest are isotropic. That this is so, even if the total production of both radiations is nearly isotropic (Murray, 1968), is not necessarily evident and may pose some problem.

Also, no correction has been made for the Doppler shift in the Balmer alpha radiation, but this can be shown to be small. The maximum angle of emission at which a Balmer alpha photon can be seen with this apparatus is about 35°. The Doppler shift for 6563A radiation at this angle for a velocity of 2.5×10^8cm/sec (maximum used) is 25A. Reference to Figure 8 shows that even this amount of shift does not seriously affect the transmission of the radiation through the filter. The maximum error estimated for this effect is 2%.

No corrections are applied to N_R, N_H, or N_N to account for dead time loss pulses through the electronice since any correction to N_H and N_N cancels with the same correction that would have to be made in N_R.

The random error in the measured cross section due to all effects is indicated in the results (next chapter) by error bars which represent the 70% confidence limit E. The total estimated systematic error is 45% at the lower velocities and 55% at the higher velocities. The random error in G is the same as for the cross section, but the systematic error is reduced to 35% since the error due to the P_{3p}, P_{3d} averaging is not present.

CHAPTER V

RESULTS AND DISCUSSION

a) Balmer Alpha and 3914 Cross Sections

The result of the measurement of the effective cross section for the production of Balmer alpha emission at a distance of 17.8 cm into the collision chamber, Q, is shown in Figure 20. This quantity is used in the data reduction (previous chapter, section d), but has no physical significance by itself. In conjunction with the cross section σ_{3s}, however, the total cross section for the production of Balmer alpha emission can be synthesized by use of the expression (again see previous chapter, section d)

$$\sigma_\alpha = Q + (1 - F_{3s})\sigma_{3s}.$$

This synthesized cross section is also shown in Figure 20 along with σ_α measured by Murray, Young, and Sheridan (1966) and with preliminary results for σ_α synthesized from measurements of σ_{3s}, σ_{3p}, and σ_{3d} separately by Hughes and Doughty (1967). The value of σ_{3s} used in the present synthesis is the result of Hughes et al. (1966) and Hughes et al. (1967) and is also shown in Figure 20.

The results of these three determinations of σ_α show a considerable lack of consistency in absolute magnitude at low velocities. In the velocity range from $\sim 1.5 \times 10^8$ cm/sec to $\sim 2.4 \times 10^8$ cm/sec, the result of the present synthesis and the synthesis of Hughes and Doughty agree quite well in shape and magnitude while in the velocity range from $\sim .5 \times 10^8$ cm/sec to $\sim 1.2 \times 10^8$ cm/sec, the present result compares quite well in shape (although

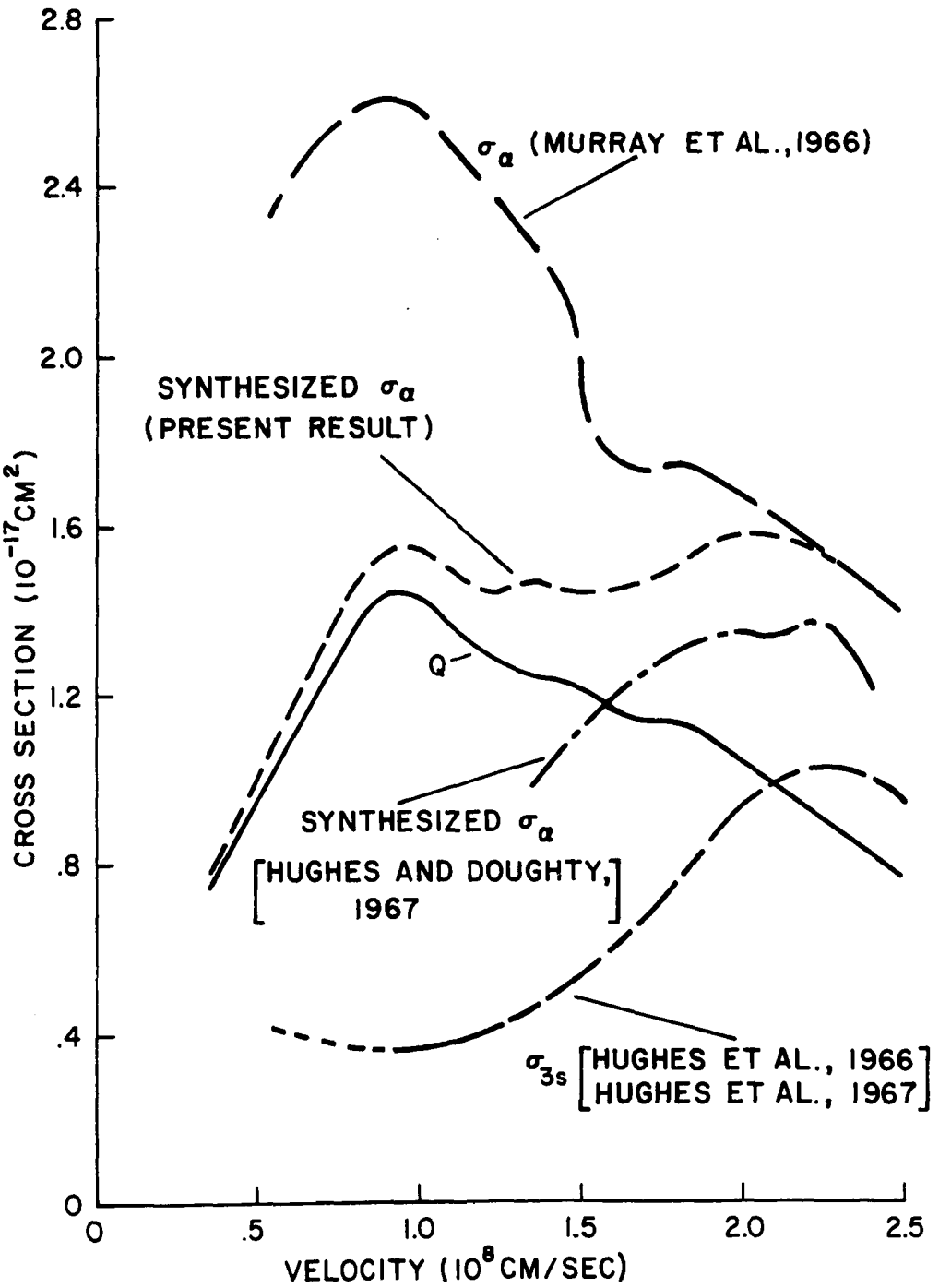

CROSS SECTIONS FOR BALMER ALPHA EMISSION

FIGURE 20

not in magnitude) with σ_α measured by Murray et al. (1966). The present result also reproduces the structural features at $.95 \times 10^8$cm/sec, 1.35×10^8cm/sec, and 1.90×10^8cm/sec reported by Murray et al. One cause of the inconsistencies at low velocities may be due to the fact that the measurements of Murray, Young, and Sheridan were taken at a long distance into the collision chamber (thereby introducing more cascade contribution) while the present measurements and Hughes' measurements are taken with relatively shorter chambers. Also, the error introduced in the present synthesis by combining results (Q and σ_{3s}) derived from calibrations at separate laboratories may be appreciable.

The result of the present measurement for σ_{3914} is shown in Figure 21. Also shown is the combined measurement of σ_{3914} by Carleton and Lawrence (1958) in the velocity range from .54 to $.88 \times 10^8$cm/sec and Sheridan, Oldenberg, and Carleton (1961) in the velocity range from .76 to 2.5×10^8cm/sec. The agreement in shape and magnitude between the present and previous measurements is exceptional, although the present result seems to decrease a little faster with increasing proton velocity than does the result of Sheridan et al.

b) $\sigma_c(3p,B) + \sigma_c(3d,B)$

The result for the sum of the cross sections $\sigma_c(3p,B)$ and $\sigma_c(3d,B)$ is shown in Figure 22. This sum increases rapidly from a value of $\sim 10^{-19}$cm^2 at a velocity of $.54 \times 10^8$cm/sec to a peak value of $\sim 1.2 \times 10^{-18}$cm^2 at a velocity of 1.15×10^8cm/sec and then decreases relatively gradually to a value of $\sim .35 \times 10^{-18}$cm^2 at a velocity of 2.4×10^8cm/sec. The random error of the individual points varies from $\sim$100% at velocities where the

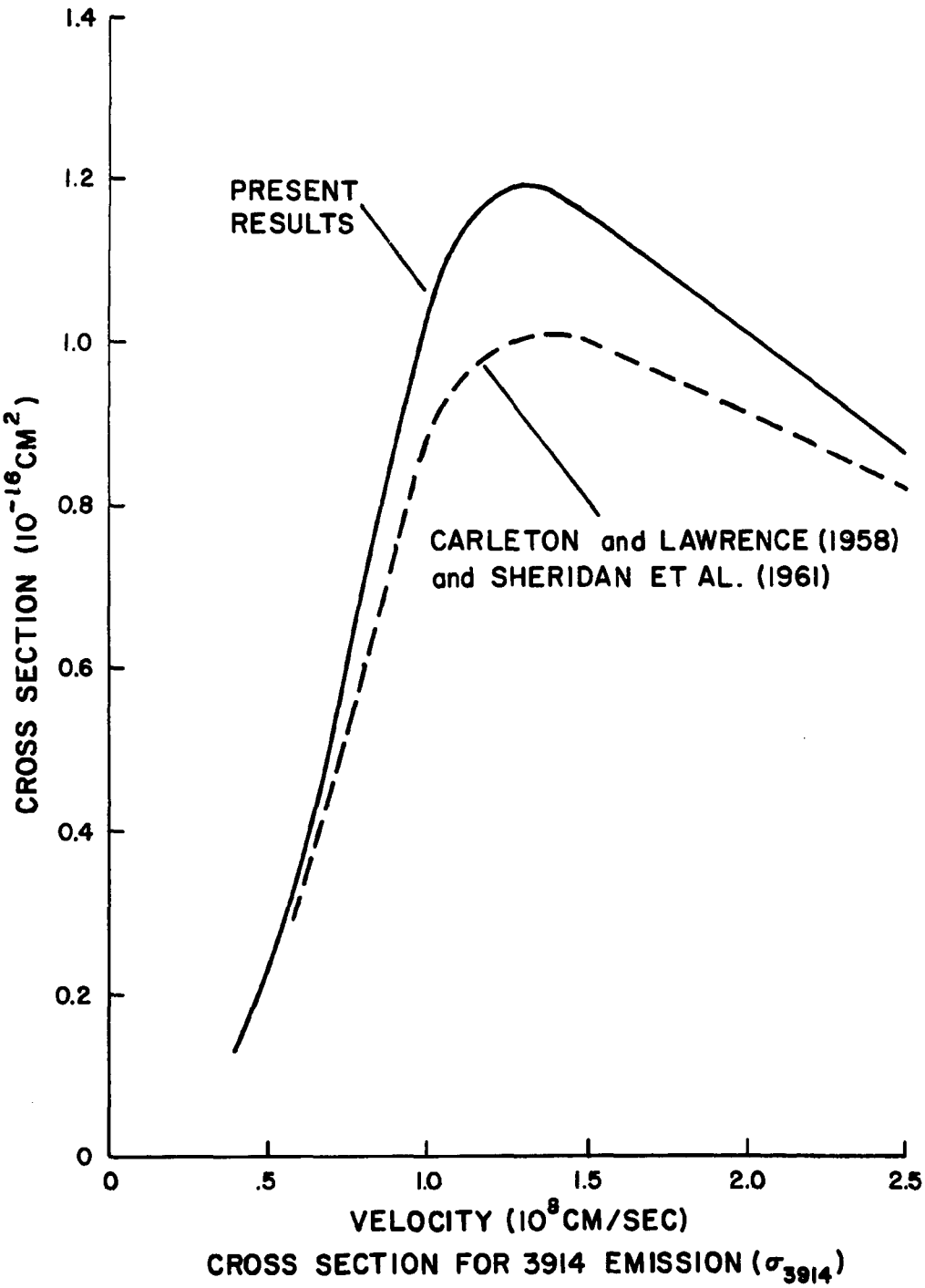

FIGURE 21

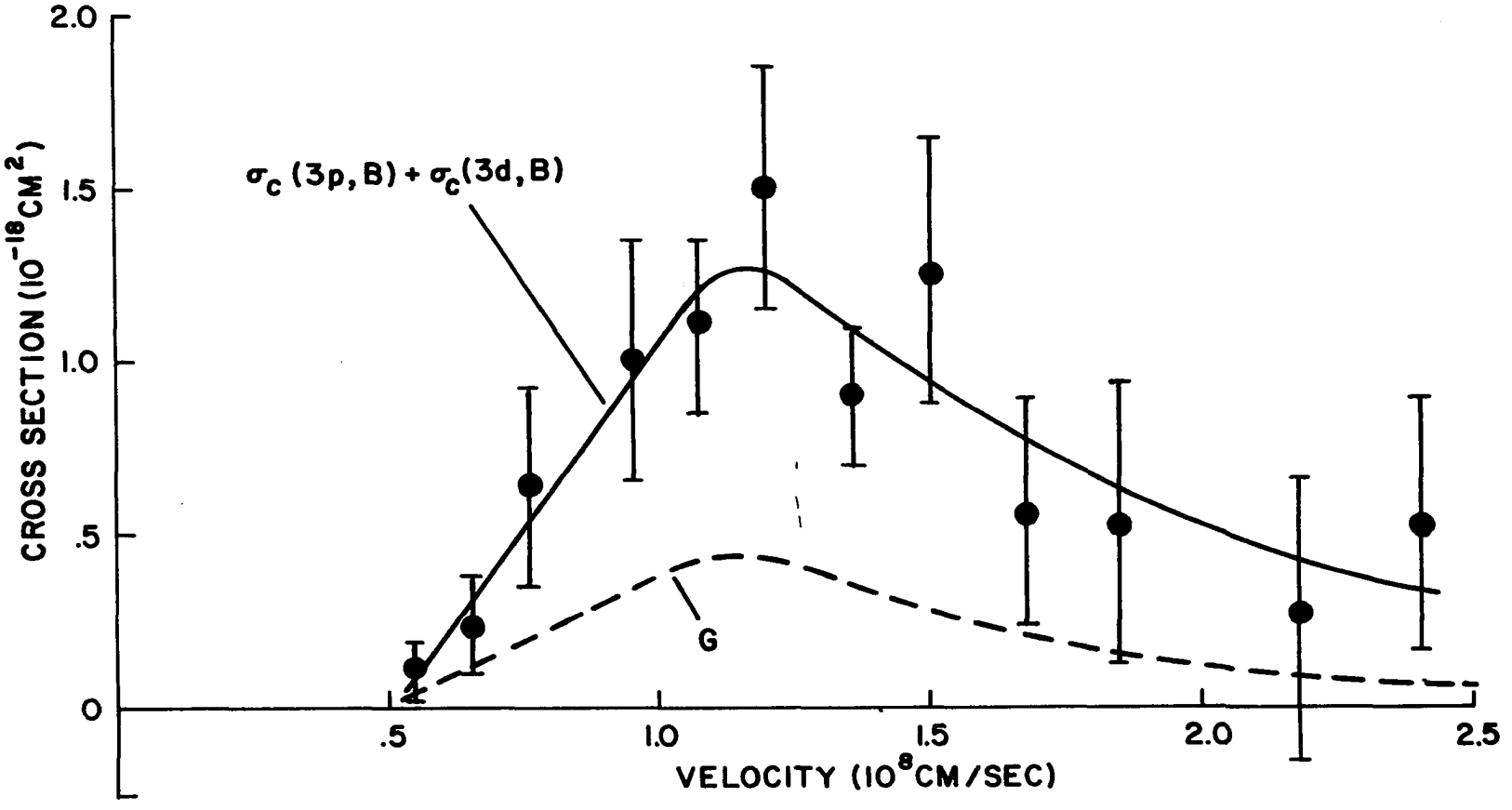

G AND σ_c (3p, B) + σ_c (3d, B)

FIGURE 22

cross section is small to ∿25% near the peak. This error is much too large to justify any statements as to structural features in the cross section other than this simple single-peak shape.

Although the sum $\sigma_c(3p,B)+\sigma_c(3d,B)$ as obtained from the measured signal by justification with the arguments of Chapter II and Chapter IV is the significant result shown in Figure 22, the value of G (see Chapter II, section e) is the quantity measured experimentally. In Chapter II (section e), G was given as

$$G = P_{3p}\sigma_c(3p,B) + P_{3d}\sigma_c(3d,B).$$

However, this is still an approximation to the signal since it neglects the 3s⟶2p and cascade contributions. The curve labeled G in Figure 22 is the experimentally measured signal reduced to dimensions of cm^2 and includes all contributions to the signal. The curve through the data points for $\sigma_c(3p,B)+\sigma_c(3d,B)$ is related to the curve for G by the relation

$$\sigma_c(3p,B) + \sigma_c(3d,B) = \frac{G}{P_e}.$$

c) Correlation between Final State Excitations

In Chapter II, sections c and f, an approximation to the shapes and relative sizes of the $\sigma_c(3m,B)$ cross sections was made by assuming that these cross sections have the same shape and relative sizes among themselves as do the total cross sections for Balmer alpha emission σ_{3m}. In other words, it was assumed that

$$\sigma_c(3m,B) = K\,\sigma_{3m}$$

where K does not depend on m. This expression may be obtained as a result in a development on the correlation between the excitation of final states of systems produced in charge exchange collisions.

Consider a charge exchange collision between a proton and an N_2 molecule in which the resulting hydrogen atom is excited to the $i^{\underline{th}}$ state and the resulting N_2^+ molecule is excited to the $j^{\underline{th}}$ state. The cross section for this process is $\sigma(i,j)$ (see Chapter I, section a). (Note: This whole following discussion is also applicable to emission rather than excitation by use of the f factors introduced in Chapter I.) The total cross sections for the excitation of the $i^{\underline{th}}$ state of hydrogen and the $j^{\underline{th}}$ state of N_2^+ are, respectively,

$$\sigma(i) = \sum_j \sigma(i,j)$$

$$\sigma(j) = \sum_i \sigma(i,j)$$

and the total charge exchange cross section is

$$\sigma_{ce} = \sum_{ij} \sigma(i,j).$$

In a large number of charge exchange collisions, the fraction of hydrogen atoms excited to the $i^{\underline{th}}$ state is

$$p_i = \frac{\sigma(i)}{\sigma_{ce}} ,$$

and the fraction of N_2^+ ions excited to the $j^{\underline{th}}$ state is

$$p_j = \frac{\sigma(j)}{\sigma_{ce}} .$$

Given that a single charge exchange collision takes place, p_i may be regarded as the probability for exciting the $i^{\underline{th}}$ state of hydrogen and p_j as the probability for exciting the $j^{\underline{th}}$ state of N_2^+. In any one collision then, the probability that the $i^{\underline{th}}$ state of hydrogen and the $j^{\underline{th}}$ state of N_2^+ are <u>both</u> excited is

$$P_{ij} = p_i p_j = \frac{\sigma(i)\sigma(j)}{\sigma_{ce}^2}$$

provided that the two excitations are <u>independent</u> events. If the two excitations are not independent, one can write

$$P_{ij} = \gamma(i,j)\,\frac{\sigma(i)\sigma(j)}{\sigma_{ce}^2}$$

where

$$\gamma(i,j) \equiv \frac{P(j|i)}{p_j} \equiv \frac{P'(i|j)}{p_i}$$

and where $P(j|i)$ is the conditional probability that the $j^{\underline{th}}$ state of N_2^+ is excited given that the $i^{\underline{th}}$ state of hydrogen is excited and $P'(i|j)$ is the similar probability for exciting the $i^{\underline{th}}$ state of hydrogen given that the $j^{\underline{th}}$ state of N_2^+ is excited. Note that $\gamma(i,j)$ is necessarily non-negative. For $\gamma(i,j) = 1$, this P_{ij} reduces to the first form obtained assuming that the two excitations are independent.

Since it is assumed that a charge exchange collision takes place, the cross section for simultaneous excitation of the $i^{\underline{th}}$ state of hydrogen and the $j^{\underline{th}}$ state of N_2^+ is

$$\sigma(i,j) = P_{ij}\sigma_{ce} = \gamma(i,j)\,\frac{\sigma(i)\sigma(j)}{\sigma_{ce}} .$$

The right-hand side of the above expression for $\sigma(i,j)$ when $\gamma(i,j) = 1$ is the cross section for exciting the $i^{\underline{th}}$ and $j^{\underline{th}}$ states of the two systems when the excitations are independent. This quantity is denoted by

$$\sigma_{uc}(i,j) = \frac{\sigma(i)\sigma(j)}{\sigma_{ce}} ,$$

and is hereafter referred to as the "uncorrelated" cross section.

Values of $\gamma(i,j)$ other than unity account for varying degrees of dependence between the two excitations. For example, if the excitation of the $i^{\underline{th}}$ state of hydrogen implies that the $j^{\underline{th}}$ state of N_2^+ <u>must</u> be excited, then $\sigma(i) \equiv \sigma(i,j)$ and

$$\gamma(i,j) = \frac{\sigma_{ce}}{\sigma(j)} ,$$

and if the excitation of the $j^{\underline{th}}$ state of N_2^+ implies that the $i^{\underline{th}}$ state of hydrogen <u>must</u> be excited, then $\sigma(j) \equiv \sigma(i,j)$ and

$$\gamma(i,j) = \frac{\sigma_{ce}}{\sigma(i)} .$$

If the excitation is such that $i \Leftrightarrow j$, then $\sigma(i,j) \equiv \sigma(i) \equiv \sigma(j)$ and

$$\gamma(i,j) = \frac{\sigma_{ce}}{\sigma(i,j)} .$$

If the simultaneous excitation of the $i^{\underline{th}}$ and $j^{\underline{th}}$ states of the two systems is for some reason forbidden, then $\gamma(i,j)$ is zero.

Although these special cases of correlation may be somewhat artificial, they do give an indication as to the possible values of $\gamma(i,j)$ for a particular pair of states (i,j) when $\sigma(i)$, $\sigma(j)$, and σ_{ce} are known.

The function $\gamma(i,j)$ may be related to a correlation function, C, which takes on values from -1 to +1 by the correspondence: $\gamma = 0 \Rightarrow C = -1$; $\gamma = 1 \Rightarrow C = 0$; and $\gamma = \sigma_{ce}/\sigma(i,j) \Rightarrow C = +1$. A value of $\gamma(i,j)$ less than unity implies a negative correlation between the indicated states while a value of $\gamma(i,j)$ greater than unity implies a positive correlation.

So far, the discussion has been concerned with the correlation between the excitation of the particular state i of hydrogen and the particular state j of N_2^+. A relation on the manifold of $\gamma(i,j)$ values resulting from a consideration of the dependence between the excitation of all the states of hydrogen with all the states of N_2^+ can be obtained. Summing both sides of the expression (which holds for a specified i and j)

$$\sigma(i,j) = \gamma(i,j)\,\frac{\sigma(i)\sigma(j)}{\sigma_{ce}}$$

over all states of both systems, one obtains immediately

$$\sigma_{ce} = \sum_{ij} \gamma(i,j)\,\frac{\sigma(i)\sigma(j)}{\sigma_{ce}} \quad .$$

But also,

$$\sigma_{ce} = \sum_{ij} \frac{\sigma(i)\sigma(j)}{\sigma_{ce}} \quad ,$$

and hence

$$\sum_{ij} [1-\gamma(i,j)]\sigma(i)\sigma(j) \geq 0.$$

A value of unity for $\gamma(i,j)$ associated with every pair (i,j) is one obvious solution of the above identity. If $\gamma(i,j)$ is greater than unity for some pairs (positive correlation), then (since both $\sigma(i)$ and $\sigma(j)$ are ≥ 0) in order to satisfy the identity, $\gamma(i,j)$ must be less than unity (negative correlation) for other pairs.

A theoretically important situation in which $\gamma(i,j)$ is unity for all pairs (i,j) occurs if there is no correlation between any of the final state excitations of the two systems--that is, if the state to which the hydrogen atom is excited is in no way influenced by the state to which the N_2^+ ion is excited, and vice versa. This means that in a large number of charge exchange collisions, the fractional distribution over the possible final states of one system is independent of the specification of the final state of the other system and that this distribution is a function of proton energy only according as the cross sections for exciting the various final states vary with energy. Note, however, that a measurement (or some other determination) of a $\gamma(i,j)$ value of unity for a particular pair (i,j) does not imply a lack of correlation among <u>all</u> of the final state excitations of the two systems.

This independence of final state excitations is the condition found by Kessel and Everhart (1966) for final charge state correlations in Ar^+-on-Ar collisions except under certain conditions in which the inelastic energy loss, Q, of the reaction displays a "triple peaked" structure. In this work, the correlation between several final charge states of each of the product systems is determined and suggests strongly that there is

a lack of correlation among all final state excitations for the argon ionization-scattering reaction.

If it is assumed that $\gamma(i,j)$ is not equal to unity for all pairs (i,j) and that it has its strongest dependence on the energy defect, ΔE, associated with the (i,j) excitation (aside from conditions which forbid the reaction), it might be reasonable to assume that $\gamma(i,j)$ decreases with increasing ΔE. Coupling this assumption with the fact that if some $\gamma(i,j)$ are greater than unity, then others must be less than unity, leads to the conclusion that those $\gamma(i,j)$ for which i and j are (or are near) the ground states must be greater than unity. However, an analysis of the Born approximation data calculated by Mapleton (1961) for simultaneous excitation of hydrogen and He^+ states in charge exchange collisions of protons on He shows that the $\gamma(i,j)$ values for (i,j) near the ground state are unity to within 10% for most (i,j) pairs. These values could presumably be even closer to unity if data for higher states were available. (That is, $\sigma(i)$ and $\sigma(j)$ are determined by summing only out to the 2p state in He^+ and to the 3d state in H). Since the value of $\Delta E(i,j)$ varies most rapidly with i and j when i and j are near the ground state of the respective systems, one consequence of this analysis is that the $\gamma(i,j)$ do not depend on ΔE. Another result of the analysis has already been stated--all the $\gamma(i,j)$ calculated are unity.

Another consequence of the assumption that the $\gamma(i,j)$ depend only on ΔE is that the $\gamma(i,j)$ would be equal for i=3s, 3p, and 3d (and j=B) since these levels are all of nearly the same energy. This in fact leads directly to the first equation of this section by setting

$$K = \frac{\gamma(3m,B)\ f_B\sigma(B)}{\sigma_{ce}} .$$

d) Calculation of $\gamma(3p+3d,B)$

The modification of the expression

$$\sigma(i,j) = \gamma(i,j)\ \frac{\sigma(i)\sigma(j)}{\sigma_{ce}}$$

to apply to the present investigation is

$$\sigma_c(3p,B) + \sigma_c(3d,B) = \gamma(3p+3d,B)\ \frac{(\sigma_{3p}+\sigma_{3d})\sigma^{ce}_{3914}}{\sigma_{ce}} .$$

Here it is assumed that γ is the same for the 3p and 3d excitations. Then, $\gamma(3p+3d,B) \equiv \gamma(3p,B) = \gamma(3d,B)$. The uncorrelated cross section (the right-hand side of the above equation with $\gamma=1$) may be written

$$\sigma_{uc} = \frac{(Q-F_{3s}\sigma_{3s})\sigma_{3914}}{\sigma_{ce}}\left[\frac{1}{1+\sigma^{i}_{3914}/\sigma^{ce}_{3914}}\right] .$$

This cross section is shown in Figure 24 along with the experimental data points for $\sigma(3p,B)+\sigma(3d,B)$. The results of the present investigation are used for Q and σ_{3914} (Figures 20 and 21), and the result of Hughes et al. (1966) and Hughes et al. (1967) for σ_{3s}. (The broken line extension of Hughes' σ_{3s} shown in Figure 20 is the extrapolation used to calculate σ_{uc} at low velocities.) The value of $\sigma^{i}_{3914}/\sigma^{ce}_{3914}$ is determined by assuming that the ratio of the number of N_2^+ molecules formed by ionization to the number formed by charge exchange is independent of the specification of the final state of N_2^+. Then

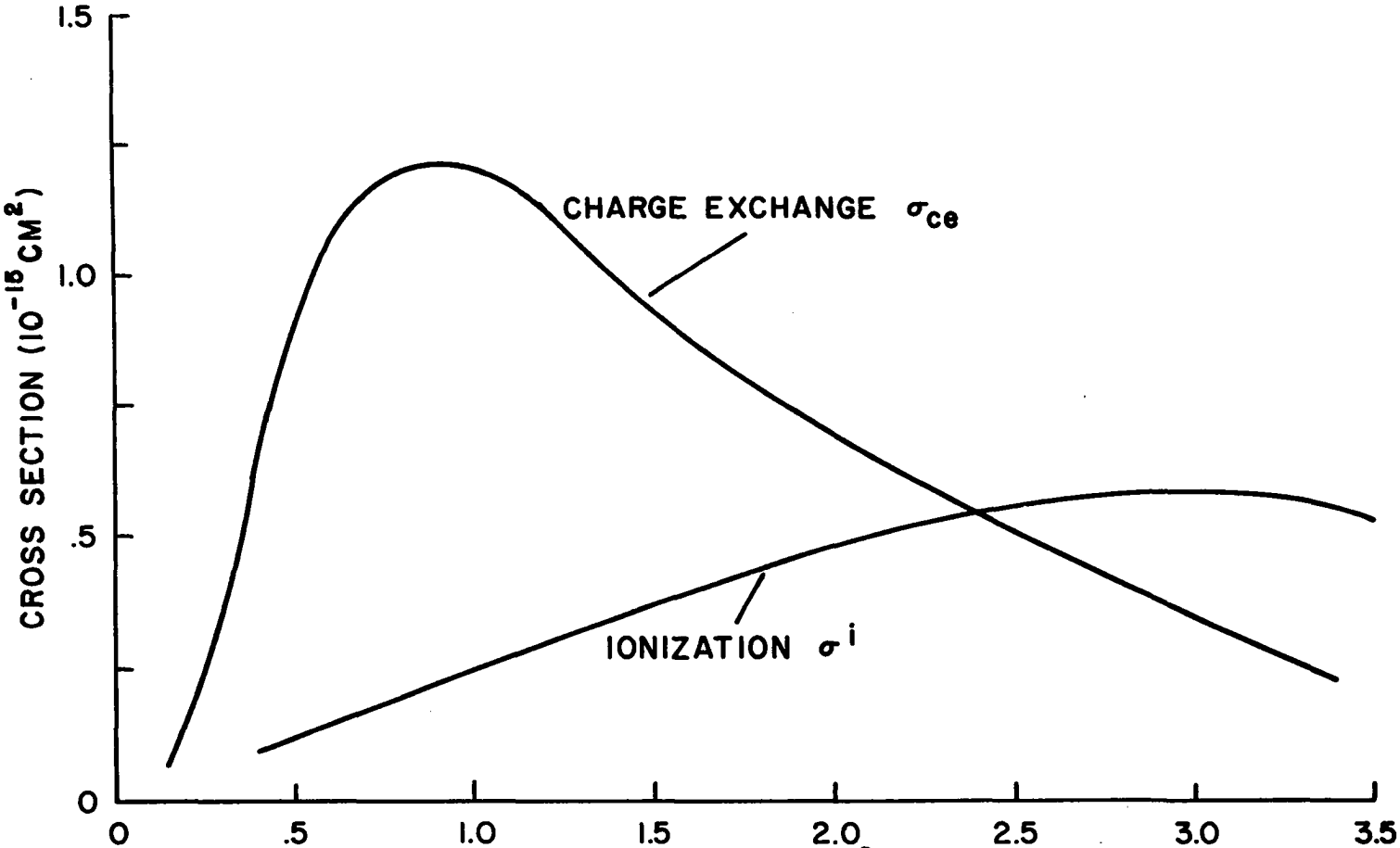

TOTAL IONIZATION AND CHARGE EXCHANGE CROSS SECTIONS

FIGURE 23

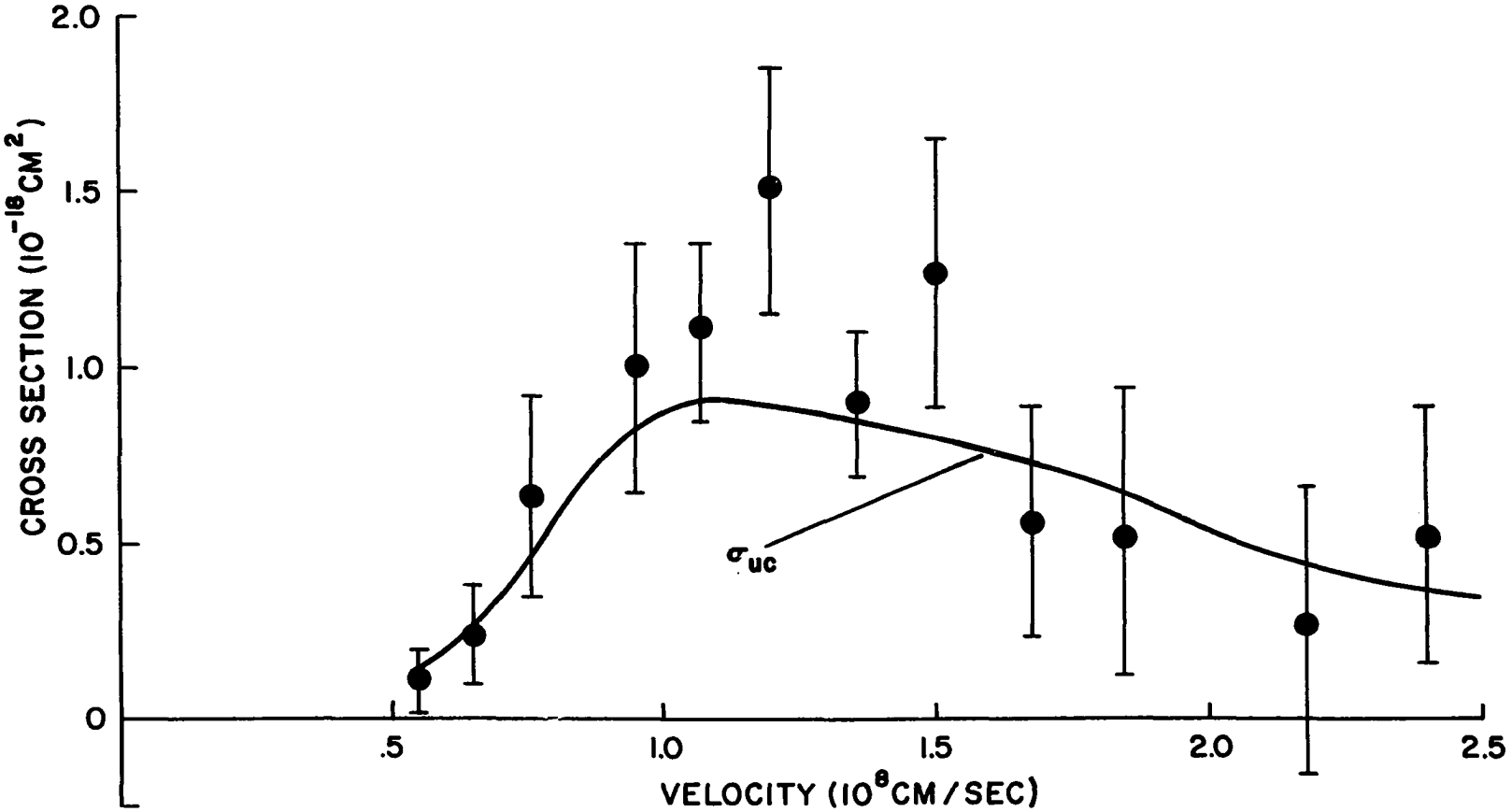

COMPARISON OF σ_{uc} WITH $\sigma_c(3p,B) + \sigma_c(3d,B)$

FIGURE 24

$$\frac{\sigma^{i}_{3914}}{\sigma^{ce}_{3914}} = \frac{\sigma^{i}}{\sigma_{ce}} \quad ,$$

where σ^{i} is the total cross section for the production of N_2^+ ions in ionization collisions of protons on N_2. The values of σ^{i} and σ_{ce} used to evaluate σ_{uc} are shown in Figure 23. σ_{ce} is an average of the cross sections reported by Carleton and Lawrence (1958), Gordeev and Panov (1964), DeHeer et al. (1966), Sheridan et al. (1961), Stier and Barnett (1956) and, except near the maximum, Gilbody and Hasted (1957). σ^{i} is an average of the cross sections reported by Sheridan et al. (1961), Gordeev and Panov (1964), DeHeer et al. (1966), and Solov'ev et al. (1962). Both of these averaged measured cross sections include contributions from reactions producing recoil particles other than N_2^+ (N^+ and N^{++} for example). However (since it is the ratio of the two cross sections that is used here), if the fractional contribution to the ionization and charge exchange cross sections caused by this effect are comparable, little error results by including the contributions. The results of Solov'ev et al. (1962) give that the contribution to the cross section for the production of slow ions (that is, the sum of the ionization and charge exchange cross sections) by recoil particles other than N_2^+ is less than $\sim$15% of the total contribution.

The estimated errors for the quantities appearing in σ_{uc} are: 10% for σ_{ce} (and $\sim$10% because of reactions producing recoil particles other than N_2^+), 15% for σ^{i}, 20% for Q and σ_{3914}, and 50% for σ_{3s}. No data are available for estimating the error associated with the approximation for $\sigma^{i}_{3914}/\sigma^{ce}_{3914}$.

The values of γ obtained from the data points for the measured cross section and this uncorrelated cross section by the relation

$$\gamma = \frac{\sigma_c(3p,B)+\sigma_c(3d,B)}{\sigma_{uc}}$$

are all unity to within experimental and approximation errors. The average value of these 12 values for γ is 1.11 with a standard deviation of .34.

e) Summary and Conclusions

As has already been stated, a measured value of γ=1 for only one pair of final state excitations in charge exchange collisions does not necessarily imply a lack of correlation among all excitations of the two systems. However, because the two states chosen for study here were selected rather arbitrarily (other than the consideration that the two emissions were chosen in the visible region of the spectrum to facilitate observation and that the cross sections for exciting these emissions are relatively large), there is a strong indication that the lack of correlation among all final states of the two systems is indeed a physical reality. The results of Kessel and Everhart and Mapleton provide further confirmation of this hypothesis. Although these two works and the present investigation consider three separate collison processes, the one physical feature common to all is that the energies of the impacting particles are well above the threshold energies for the excitation processes investigated. The lack of correlation in all three processes might well be understood then in terms of a general model (such as the one presented by

Russek, 1963) in which the incoming systems form an intermediate combined excited system; the energy of this intermediate system is shared between the excited final systems; and the two final systems are left (after parting) to do whatever they will, independently of each other.

The primary significant conclusion of the present investigation is that it provides evidence for the lack of correlation between final state excitations in collisions where the impact energy is well above the threshold energy for the process under consideration.

A practical consequence of uncorrelated final state excitations (which has already been used in the calculation of σ_{uc}) is that the fundamental cross sections $\sigma(i,j)$ can be calculated knowing only the total cross sections $\sigma(i)$, $\sigma(j)$, and σ_{ce}. Another significant point is that if there is a lack of correlation, theoretical investigations of charge exchange collisions must predict this effect. (The Born approximation calculation of Mapleton displays this lack of correlation.)

Aside from the significance of final state excitation correlations, the fact that the technique of photon-photon coincidence measurements has been shown to be a realizable method for gaining information about the fundamentals of atomic and molecular excitation reactions is highly pertinent. The measurements carried out here are the first of their kind in which an emission cross section is determined for a "specific" excitation-emission reaction (leaving aside the specification of the scattering).

BIBLIOGRAPHY

Afrosimov, V. V., Gordeev, Yu. S., Panov, M. N., and Fedorenko, N. V., "Investigation of Atomic Collisions by a Coincidence Technique," Soviet Physics - Tech. Phys. 9, 1248(1965).

Bates, D. R., and Dalgarno, A., "Electron Capture-III: Capture into Excited States in Encounters between Hydrogen Atoms and Fast Protons," Proc. Phys. Soc. 66, 972(1958).

Bennett, R. G., and Dalby, F. W., "Experimental Determination of the Oscillator Strength of the First Negative Bands of N_2^+," J. Chem. Phys. 31, 434(1959).

Bethe, H. A., and Salpeter, E. E., "Quantum Mechanics of One- and Two-Electron Systems," Encyclopedia of Physics, Vol. XXXV, Springer-Verlag, Berlin, 1957, p. 376.

Bobashev, S. V., Andreev, E. P., and Ankudinov, V. A., "Excitation of Balmer Hydrogen Lines upon Passage of H^+, H_2^+, and H_3^+ through Helium and Neon," Soviet Physics - JETP 18, 1205(1964).

Bogdanova, I. P., and Marusin, V. D., "Study of the Secondary Processes due to Electronic Excitation using the Coincidence Count Method," Optics and Spectroscopy 20, 113(1966).

Carleton, N. P., "Excitation of Nitrogen by Protons of a Few KeV Energy," Phys. Rev. 107, 110(1957).

Carleton, N. P., and Lawrence, T. R., "Absolute Cross Sections for Excitation of Nitrogen by Protons of a Few KeV Energy," Phys. Rev. 109, 1159(1958).

Condon, E. U., and Shortley, G. H., The Theory of Atomic Spectra, Cambridge University Press, London, 1963, p. 136.

Cristofori, F., Fenici, P., Frigerio, G. E., Molho, N., and Sona, P. G., "Single Photon Coincidence Method for the Absolure Measure of the Efficiency of a 1216A Detector," Physics Letters 6, 171(1963).

Dahlberg, D. A., Anderson, D. K., and Dayton, I. E., "Optical Emissions Produced by Proton and Hydrogen-Atom Impact on Nitrogen," Phys. Rev. 164, 20(1967).

DeHeer, F. J., Schutten, J., and Moustafa, H., "Ionization and Electron Capture Cross Sections for Protons Incident on Noble and Diatomic Gases between 10 and 140 KeV," Physica 32, 1766(1966).

Gilbody, H. R., and Hasted, J. B., "Anomalies in the Adiabatic Interpretation of Charge Transfer Collisions," Proc. Roy. Soc. A238, 334 (1957).

Gordeev, Yu. S., and Panov, M. N., "Ionization and Capture of Electrons during Collisions of Hydrogen Ions with Atoms and Molecules of a Gas," Soviet Physics - Tech. Phys. 9, 656(1964).

Hoel, P. G., Introduction to Mathematical Statistics, John Wiley and Sons, Inc., New York, 1962, p. 275.

Hughes, R. H., Dawson, H. R., and Doughty, B. M., "Electron Capture into the 4s State of H by Fast H^+ Impact on Gases," Phys. Rev. 164, 166(1967).

Hughes, R. H., Dawson, H. R., Doughty, B. M., Kay, D. B., and Stigers, C. A., "Electron Capture into the 3s State of Hydrogen by Fast-Proton Impact on Gases," Phys. Rev. 146, 53(1966).

Hughes, R. H., and Doughty, B. M., Private Communications, (1967).

Kessel, Q. C., and Everhart, E., "Coincidence Measurements of Large-Angle Ar^+-on-Ar Collisions," Phys. Rev. 146, 16(1966).

Mapleton, R. A., "Electron Capture from $He(1s^2)$ by Protons," Phys. Rev. 122, 528(1961).

Melissinos, A. C., Experiments in Modern Physics, Academic Press, New York, 1966, p. 407.

Murray, J. S., "Excitation Functions for Balmer and N_2^+ First Negative Emissions Produced in Collisions of Protons with $^2N_2$," dissertation, University of Alaska, 1968.

Murray, J. S., Young, S. J., and Sheridan, J. R., "Cross Section and Polarization of Balmer-Alpha Radiation Produced in Charge-Exchange Collisions of Protons with N_2," Phys. Rev. Letters 16, 439(1966).

Nicholls, R. W., "Errata," J. Atmosph. Terr. Phys. 24, 749(1962).

Nicholls, R. W., "Einstein A Coefficients, Oscillator Strengths and Absolute Band Strengths for the N_2 Second Positive and N_2^+ First Negative Systems," J. Atmosph. Terr. Phys. 25, 218(1963).

Philpot, J. L., and Hughes, R. H., "Spectroscopic Study of Controlled Proton Impact on Molecular Nitrogen," Phys. Rev. 133, A107(1964).

Russek, A., "Ionization Produced by High-Energy Atomic Collisions," Phys. Rev. 132, A246(1963).

Sheridan, J. R., and Clark, K. C., "Vibration and Rotation of N_2^+ Excited by 10-65-KeV Ions," Phys. Rev. 140, A1033(1965).

Sheridan, W. F., Oldenberg, O., and Carleton, N. P., "Excitation of Nitrogen by Controlled Proton and Electron Impact," 2nd Int. Conf. on the Physics of Electronic and Atomic Collisions; Abstract of Papers, W. A. Benjamin Inc., New York, 1961, p. 159.

Skachkov, Yu. F., "Investigation of the Time Correlation of Photons Emitted in NeII Spectral Lines of Separate Neon Atoms Excited by Electron Impact," Soviet Physics - JETP 19, 804(1964).

Solov'ev, E. S., Il'lin, V. A., Oparin, V. A., and Fedorenko, N. V., "Ionization of Gases by Fast Hydrogen Atoms and by Protons," Soviet Physics - JETP 15, 459(1962).

Stier, P. M., and Barnett, C. F., "Charge Exchange Cross Section of Hydrogen Ions in Gases," Phys. Rev. 103, 896(1956).

Wallace, L. V., and Nicholls, R. W., "The Interpretation of Intensity Distributions in the N_2 Second Positive and N_2^+ First Negative Band Systems," J. Atmosph. Terr. Phys. 7, 101(1955).